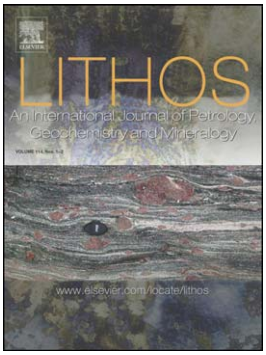

Clinopyroxene-melt element partitioning during interaction between trachybasaltic magma and siliceous crust: Clues from quartzite enclaves at Mt. Etna volcano

S. Mollo, J.D. Blundy, P. Giacomoni, M. Nazzari, P. Scarlato, M. Coltorti, A. Langone, D. Andronico

PII: S0024-4937(17)30177-9
DOI: doi:10.1016/j.lithos.2017.05.003
Reference: LITHOS 4310

To appear in: *LITHOS*

Received date: 3 February 2017
Accepted date: 7 May 2017

Please cite this article as: Mollo, S., Blundy, J.D., Giacomoni, P., Nazzari, M., Scarlato, P., Coltorti, M., Langone, A., Andronico, D., Clinopyroxene-melt element partitioning during interaction between trachybasaltic magma and siliceous crust: Clues from quartzite enclaves at Mt. Etna volcano, *LITHOS* (2017), doi:10.1016/j.lithos.2017.05.003

Clinopyroxene-melt element partitioning during interaction between trachybasaltic magma and siliceous crust: Clues from quartzite enclaves at Mt. Etna volcano

S. Mollo[1], J. D. Blundy[2], P. Giacomoni[3], M. Nazzari[4], P. Scarlato[4], M. Coltorti[3], A. Langone[5], D. Andronico[4]

[1]Dipartimento di Scienze della Terra, Sapienza-Università di Roma, P.le Aldo Moro 5, 00185 Roma, Italy

[2]School of Earth Sciences, University of Bristol, Wills Memorial Building, Bristol BS8 1RJ, UK

[3]Dipartimento di Fisica e Science della Terra, Università di Ferrara, Via Saragat 1, 44122 Ferrara, Italy

[4]Istituto Nazionale di Geofisica e Vulcanologia, Via di Vigna Murata 605, 00143 Rome, Italy

[5]C.N.R.-Istituto di Geoscienze e Georisorse, UOS Pavia, Via Ferrata 1, 27100 Pavia, Italy

Corresponding author:

Silvio Mollo

Sapienza-Università di Roma

Dipartimento di Scienze della Terra

P.le Aldo Moro 5

00185 Roma, Italy

e-mail silvio.mollo@uniroma1.it

Abstract

A peculiar characteristic of the paroxysmal sequence that occurred on March 16, 2013 at the New South East Crater of Mt. Etna volcano (eastern Sicily, Italy) was the eruption of siliceous crustal xenoliths representative of the sedimentary basement beneath the volcanic edifice. These xenoliths are quartzites that occur as subspherical bombs enclosed in a thin trachybasaltic lava envelope. At the quartzite-magma interface a reaction corona develops due to the interaction between the Etnean trachybasaltic magma and the partially melted quartzite. Three distinct domains are observed: (i) the trachybasaltic lava itself (Zone 1), including Al-rich clinopyroxene phenocrysts dispersed in a matrix glass, (ii) the hybrid melt (Zone 2), developing at the quartzite-magma interface and feeding the growth of newly-formed Al-poor clinopyroxenes, and (iii) the partially melted quartzite (Zone 3), producing abundant siliceous melt. These features makes it possible to quantify the effect of magma contamination by siliceous crust in terms of clinopyroxene-melt element partitioning. Major and trace element partition coefficients have been calculated using the compositions of clinopyroxene rims and glasses next to the crystal surface. Zone 1 and Zone 2 partition coefficients correspond to, respectively, the chemical analyses of Al-rich phenocrysts and matrix glasses, and the chemical analyses of newly-formed Al-poor crystals and hybrid glasses. For clinopyroxenes from both the hybrid layer and the lava flow expected relationships are observed between the partition coefficient, the valence of the element, and the ionic radius. However, with respect to Zone 1 partition coefficients, values of Zone 2 partition coefficients show a net decrease for transition metals (TE), high-field strength elements (HFSE) and rare earth elements including yttrium (REE+Y), and an increase for large ion lithophile elements (LILE). This variation is associated with coupled substitutions on the M1, M2 and T sites of the type $^{M1}(Al, Fe^{3+}) + {}^{T}Al = {}^{M2}(Mg, Fe^{2+}) + {}^{T}Si$. The different incorporation of trace elements into clinopyroxenes of hybrid origin is controlled by cation substitution reactions reflecting local charge-balance requirements. According to the lattice strain theory, simultaneous cation exchanges across the M1, M2, and T sites have profound effects on REE+Y and HFSE partitioning. Conversely, both temperature and melt

composition have only a minor effect when the thermal path of magma is restricted to ~70 °C and the value of non-bridging oxygens per tetrahedral cations (NBO/T) shifts moderately from 0.31 to 0.43. As a consequence, Zone 2 partition coefficients for REE+Y and HFSE diverge significantly from those derived for Zone 1, accounting for limited cation incorporation into the newly-formed clinopyroxenes at the quartzite-magma interface.

Keywords: clinopyroxene-melt element partitioning, magma contamination, quartzite xenoliths, Mt. Etna volcano.

1. Introduction

Mafic magmatism is generally invoked as the primary agent of crustal melting processes associated with a wide spectrum of contaminated magmas (Grove et al., 1988; Bergantz and Dawes, 1994; Mollo et al., 2011; Mollo and Vona, 2014). During early stages of contamination, rates of crustal assimilation can substantially exceed those of crystallization, with remarkable effects on trace element concentrations and isotopic evolution of magma (Huppert and Sparks, 1985; Reiners et al., 1995). Interpreting the geochemical compositions of mafic magmas depends on recognizing that their passage through a lithologically heterogeneous crust presents opportunities for assimilation of crustal materials via open-system processes. Under such circumstances, the degree of contamination is dictated by magma and crust compositions, temperature, incubation time, and rate of magma supply (Hildreth and Moorbath, 1988; Huppert and Sparks, 1988; Kerr et al., 1995; Cribb and Barton, 1996; Gamble et al., 1999; Dungan and Davidson, 2004; Erdmann et al., 2007).

The occurrence of xenocrysts and xenoliths in lavas indicate that assimilation of crustal lithologies is a dynamic process characterized by multiple stages and mechanisms of dissolution (i.e., mechanical disaggregation and partial melting) leading to formation of contaminated melts and refractory xenocrysts. Digestion of xenoliths in mafic magmas may be extraordinarily rapid with the potential to impose significant geochemical overprints on host magmas due to mixing with anatectic

melts (Costa and Dungan, 2005; Erdmann et al., 2007). Xenoliths in trachybasaltic lavas at Mt. Etna volcano (eastern Sicily, Italy) display mineralogical and geochemical changes associated with partial-to-complete melting of crustal materials that contribute to selective alkali enrichments in the enclosing magma (Michaud, 1995). An interesting peculiarity of siliceous xenoliths is the development of high-temperature reaction coronas at the xenolith-magma interface in which distinctive clinopyroxenes crystallize from differentiated alkaline melts of hybrid origin (Michaud and Clocchiatti, 1995). This study attempts to quantify the geochemical effect of magma contamination by siliceous crust in terms of clinopyroxene-melt element partitioning. Although the discussion is limited in scope to the partial melting of quartzite xenoliths, the overall geochemical characteristics of natural products are relevant to other situations that involve mixing between SiO_2-rich anatectic melts and trachybasaltic magmas. These contamination phenomena favor the crystallization of diopside-rich clinopyroxenes compositionally distinct from those resulting from closed-system differentiation of the host magma. Thermodynamic considerations based on the lattice strain theory show that trace element partitioning is controlled primarily by abrupt changes in clinopyroxene chemistry, whereas minor effects can be attributed to temperature and melt composition at the conditions observed in this study. Melt hybridization processes accompanied by clinopyroxene crystallization cause unexpected trace element partitioning with respect to changes observed during magma differentiation by either fractional crystallization or assimilation and fractional crystallization (AFC) mechanisms.

2. Geological background

Mt. Etna, the most active basaltic volcano in Europe, developed in a complex tectonic context at the intersection of tensional tectonic fractures that cut a 10-15 km-thick sedimentary-metamorphic pile, composed of two main structural units: the autochthonous carbonate unit of the Hyblean Plateau (the undeformed foreland domain of the African continental plate margin) and the overlying allochthonous flysch series of the Apenninic-Maghrebian Chain (Branca et al., 2011).

The onset of volcanism occurred with the eruption of tholeiitic basalts (ca. 500 ka) and, subsequently (ca. 220 ka), the composition of magmas shifted towards a more alkaline affinity (Tanguy et al., 1997). Volcanic activity is characterized by common summit eruptions and less frequent flank eruptions that are both controlled principally by rapid magma ascent and decompression along a vertically-developed central conduit (Corsaro et al., 2009). A distinctive feature of the recent activity is the relatively constant degree of magmatic differentiation with systematic eruption of trachybasaltic magmas containing a uniform phenocryst assemblage of olivine, clinopyroxene, plagioclase, and titanomagnetite (Ferlito et al., 2011; Armienti et al., 2013; Lanzafame et al., 2013; Mollo et al., 2013a; Giacomoni et al., 2014). The plumbing system is governed by frequent inputs from mantle depths of primitive, volatile-rich magmas that mix with more evolved, degassed melts residing at shallow crustal levels (Clocchiatti et al., 2004; Métrich et al., 2004; Spilliaert et al., 2006; Ferlito et al., 2008; Mollo et al., 2011a; Kahl et al., 2015).

During the January 2011 - April 2013 paroxysmal sequence at Mt. Etna, the New South East Crater of the volcano was characterized by several episodes of lava fountaining (Behncke et al., 2014; Viccaro et al., 2015). The trachybasaltic scoria clasts from these events show the typical phase assemblage of Etnean eruptions, with porphyritic index ranging between 15 and 30 vol.%. Both crystals and host magmas were rapidly quenched at the contact with the atmosphere, preserving the original compositions attained under intratelluric conditions (Mollo et al., 2015a). The crystallization path of magmas feeding the lava fountains has been estimated using the compositions of clinopyroxenes phenocrysts and matrix glass from scoria clasts as input data for thermometers, barometers and hygrometers (Mollo et al., 2015a; Perinelli et al., 2016). The estimates indicate that the saturation temperature of clinopyroxene decreases from ~1,150 to ~1,050 °C along a decompression path from ~800 to ~0.1 MPa in which the melt-H_2O concentration decreases from ~4.5 to ~1.5 wt.%. Changes in the *P*-*T*-H_2O crystallization conditions of clinopyroxene reflect the shift from H_2O-undersaturated to H_2O-saturated regimes (Armienti et al., 2013). Volatile-rich magmas stored in the deeper parts of the plumbing system are persistently

buffered to the composition of trachybasalt by low degrees of fractional crystallization in the order of 10-20 vol.% (Corsaro et al., 2013; Mollo et al., 2015b; Vetere et al., 2015). Conversely, at shallower crustal levels, Etnean magmas undergo strong degassing and crystallization while travelling from the conduit to the surface (Métrich et al., 2004; Spilliaert et al., 2006). On eruption, the phenocryst and microphenocryst content of magma is up to 50 vol.% but a great number of crystals nucleate and grow by degassing- and cooling-driven crystallization mechanisms (Applegarth et al., 2013).

A peculiar characteristic of the paroxysmal sequence on March 16, 2013 at Etna's New South East Crater was the eruption of siliceous crustal xenoliths representative of the sedimentary basement beneath the volcano. These xenoliths are quartzites from the stratigraphic formations (i.e., sands, sandstones, quartzites, and quartz arenites) of the Sicilide Tectonic Unit (~3 km depth, ~100 MPa lithostatic pressure) belonging to the Apenninic-Maghrebian Chain (Branca et al., 2011). Both crustal (Michaud, 1995) and cognate (Corsaro et al., 2014) xenoliths are commonly found in the prehistoric and historic Etnean eruptions as heralds of shallow-to-deep interaction processes between sedimentary, metamorphic, or igneous rocks and ascending trachybasaltic magmas. Additionally, changes in the physico-chemical properties of silicate and carbonate sedimentary rocks under the effect of thermally-induced reactions are addressed as source of (i) anomalously low seismic velocity zones at depth (Mollo et al., 2011), (ii) volcanic edifice instability mechanisms (Mollo et al., 2012a), (iii) extremely high H_2O (silicate mineral dehydroxylation) and CO_2 (carbonate mineral decarbonation) emissions (Michaud, 1995; Mollo et al., 2011; Heap et al., 2013) and (iv) selective contamination of the magma with enrichments in K, Rb and Cs by percolation of a carrier fluid phase through the upper part of the magmatic feeding system (Michaud, 1995).

3. Analytical methods

Textural and microchemical analyses were carried out at the HP-HT Laboratory of Experimental Volcanology and Geophysics of the Istituto Nazionale di Geofisica e Vulcanologia in

Rome (Italy). Images were collected in backscattered electron (BSE) mode of a field emission gun-scanning electron microscopy (FE-SEM) Jeol 6500F equipped with an energy-dispersive spectrometer (EDS) detector. Microchemical analyses (Table 1S) were performed using an electron probe micro-analyzer (EPMA) Jeol-JXA8200 with combined EDS-WDS (five spectrometers with twelve crystals). Data were collected using 15 kV accelerating voltage and 10 nA beam current. For glasses, a slightly defocused electron beam with a size of 3 μm was used, with a counting time of 5 s on background and 15 s on peak. For crystals, the beam size was 1 μm with a counting time of 20 and 10 s on peaks and background respectively. The following standards were used: jadeite (Si and Na), corundum (Al), forsterite (Mg), andradite (Fe), rutile (Ti), orthoclase (K), apatite (P), and spessartine (Mn). Sodium and potassium were analyzed first to minimize alkali migration effects. The precision of the microprobe was measured through the analysis of well-characterized synthetic oxide and mineral secondary standards. Based on counting statistics, analytical uncertainties relative to their reported concentrations indicate that precision was better than 5% for all cations. BSE imaging combined with X-ray mapping were adopted for the identification of the main textural and compositional features of each sample. X-ray maps were collected for Si, Al, Fe, Mg, and Ca by using 15 kV accelerating voltage, 8 nA probe current, resolution 1024 × 768 pixel^2, and dwell time 10 ms (real time) per pixel. To the single-band images, representing X-ray maps for Si and Al, were assigned different colors (blue and red, respectively) and combined to form a colored three-band image. Phases containing a combination of more than one of the elements being mapped are displayed with composite colors.

Trace element analyses were conducted at the CNR-IGG–Pavia by LA-ICP-MS (Laser Ablation Inductively Coupled Plasma Mass Spectrometry). The chosen trace elements are representative of the following geochemical groups (Table 1S): rare earth elements (REE) comprising both light (LREE; La, Ce, Pr, Nd, Sm, Eu, and Gd) and heavy (HREE; Tb, Dy, Ho, Er, Tm, Yb and Lu, plus Y) elements, high field strength elements (HFSE; Ti, Hf, and Zr), large-ion lithophile elements (LILE; Sr, Pb, and Ba), and transition elements (TE; Cr and Sc). The laser

source used for the analyses consists of a Q-switched Nd:YAG laser (Brilliant, Quantel), with a fundamental emission in the near-IR region (1064 nm) which is converted into 266 nm by two harmonic generators. Using mirrors, the laser beam is carried into a petrographic microscope, focused above the sample, and then projected onto it. Optimum average instrumental operating conditions are: RF power 800-900 W, cooling gas 12.08 l min^{-1}, sample gas 0.9-1.1 l min^{-1}, auxiliary gas 1.00 l min^{-1} and carrier gas 0.9-1.1 l min^{-1}. The total scan-time is about 700 ms, the settling time is about 340 ms, and hence the acquisition efficiency is estimated at about 50%. A typical analysis consists of acquiring one minute of background and one minute of ablated sample, thus approximately 170 sweeps are required. The mean integrated time for acquisition is about 0.9 s for each element. A 10 μm spot size was used for LA-ICP-MS measurements. The ablated material was analyzed with a quadrupole (DRCe, PerkinElmer). NIST-SRM610 was used as an external standard; ^{43}Ca or ^{29}Si were adopted as internal standards for clinopyroxene and glass analyses respectively. In each analytical run the USGS reference sample BCR2 was analyzed together with the unknowns for quality control. The precision of individual analyses varied depending upon a number of factors, e.g., the element and isotope analyzed as well as the chemical homogeneity of crystal and glass. However, the 1 sigma errors calculated from variations in replicate analyses of crystals and glasses were invariably several times larger than the fully integrated 1 sigma errors determined from counting statistics alone. Trace element Nernst partition coefficients [$D_i = (I)_{xls} / (I)_{melt}$ on a weight basis] were calculated using the clinopyroxene rim and coexisting glass analyses (Table 2S). To avoid contamination caused by the partial ablation of crystals, the glass was analyzed 3 μm away from the clinopyroxene edge. For the case of the trachybasaltic lava, partition coefficients (i.e., Zone 1 partition coefficients) were derived using the compositions of clinopyroxene phenocrysts and matrix glasses, as representative of the quenched melt phase supplying chemical components to the growing crystals. Conversely, for the case of the quartzite-magma interface, partition coefficients (i.e., Zone 2 partition coefficients) were derived using the

compositions of newly-formed clinopyroxenes and coexisting glasses, as representative of the hybrid melt from which crystals nucleated and grew.

Bulk rock analyses for major and trace elements, as well as oxygen isotope analyses were conducted at Actlabs (Activation Laboratories Ltd.). These analyses are reported in the supplementary material (Table 3S), together with measured and certified analyses of international reference materials. Major elements were analyzed by lithium metaborate/tetraborate fusion – ICP-OES (inductively coupled plasma optical emission spectrometry). Sample washing was performed to remove any organic, loosely adhered, and cementing material. Washing included soaking in a hot mixture of HCl and H_2O_2 as well as cleaning in acetone using ultrasound. The analyses were performed in a batch system. Each batch contained a method reagent blank, certified reference material and 17% replicates. Samples were mixed with a flux of lithium metaborate and lithium tetraborate and fused in an induction furnace. The melted material was immediately poured into a solution of 5% nitric acid containing an internal standard, and mixed continuously until completely dissolved (about 30 minutes). The samples were run on a Thermo Jarrell-Ash ENVIRO II ICP. Calibration was performed using 7 prepared USGS and CANMET certified reference materials. FeO was determined through titration, using a cold acid digestion of ammonium metavanadate, and hydrofluoric acid in an open system. Ferrous ammonium sulphate was added after digestion and potassium dichromate was the titrating agent. This cold digestion dissolved silicates and some sulphides. Water content was determined gravimetrically. About 0.3 g sample was thermally decomposed in a resistance furnace in a pure nitrogen environment at 110 °C (moisture, H_2O^-) followed by decomposition at 1,000 °C (interstitial water, H_2O^+), using an ELTRA CW-800, directly releasing H_2O. Trace elements were measured by lithium metaborate/tetraborate fusion – ICP-MS (inductively coupled plasma mass spectrometry). Samples fused as reported above were diluted and analyzed by Perkin Elmer Sciex ELAN 6000, 6100 or 9000 ICP/MS. Three blanks and five controls (three before sample group and two after) were analyzed per group of samples. Oxygen isotopes were measured by reaction with BrF_5 at about 650 °C in nickel bombs. The

fluorination reaction converts O in the minerals to O_2 gas, which is subsequently converted to CO_2 gas using a hot C rod. All reaction steps are quantitative. Isotopic analyses were performed on a Finnigan MAT Delta, dual inlet, isotope ratio mass spectrometer. Oxygen isotope ratios are reported in the standard delta notation as per mil deviations from V–SMOW (hereafter reported to as SMOW). External reproducibility is ±0.19‰ (1 sigma error).

4. Results

4.1 Textural characters

Quartzites of this study occur as subspherical bombs with maximum length of 4-15 cm enclosed in a thin trachybasaltic lava envelope (Fig. 1a; cf. Michaud, 1995). The interaction between the trachybasaltic magma and the quartzite can be represented by three distinct domains: (i) trachybasaltic lava (Zone 1; Fig. 1b,c,f), (ii) hybrid melt forming a variably thick (~50-500 μm) boundary layer between lava and quartzite (Zone 2; Fig. 1b,c,d,e), and (iii) partially melted quartzite (Zone 3; Fig. 1b,c,d,e). Zone 1 displays the typical phase assemblage found in recent trachybasaltic Etnean eruptions (cf. Mollo et al., 2015b) that, in order of abundance, comprises tabular plagioclase, prismatic clinopyroxene, subrounded olivine and titanomagnetite dispersed in a vesicular matrix glass (Fig. 1b,c,f). Zone 2 is characterized by melt hybridism associated with crystallization of clinopyroxenes chemically different from those in host lava (Fig. 1b,c,d,e). The texture of Zone 2 clinopyroxenes changes from euhedral to anhedral with maximum size (~50 μm) smaller than that (~120 μm) generally observed for Zone 1 prismatic crystals (Fig. 1f). Rarely, the hybrid melt may be thick enough so that larger (~100 μm) clinopyroxenes also occur in Zone 2, exhibiting well-formed planar edges (Fig. 1e). These texturally mature minerals may form by aggregation of smaller and mutually touching smaller crystals, resembling crystal growth mechanism documented by ex-situ (Pupier et al., 2008; Iezzi et al., 2011, 2014; Mollo et al., 2012b) and in-situ (Schiavi et al., 2009) experiments. Zone 3 is made of subrounded quartz crystal relics embedded in a vesicular interstitial glass. The size of quartz grains changes significantly from ~20

to ~700 μm (Fig. 1b,c,d,e) but most of the smaller crystals occur in close contact with the trachybasaltic host at the periphery of the subspherical bomb (Fig. 1d) where the degree of partial melting is maximum (cf. Michaud, 1995).

4.2 Clinopyroxene chemistry and crystallization

The comparison between clinopyroxenes from Zone 1 and Zone 2 reveals that crystals from the trachybasaltic lava show ^{T}Al/Si ratios (~0.1-0.13; Al and Si are expressed as atoms per formula unit) much higher than those (~0.02-0.04) measured in the hybrid melt (Fig. 2). Contrary to what is observed in Zone 2, clinopyroxenes from Zone 1 are also enriched in Ti, Fe_{tot}, Na, and Cr, counterbalanced by depletions in Mg and Ca (Fig. 2). The charge balance equation of Lindsley (1980) for the nominal determination of Fe^{3+} indicates that the Fe^{2+}/Fe^{3+} ratio of clinopyroxene increases from ~2 to ~6 from Zone 1 to Zone 2. Accordingly, clinopyroxenes from the hybrid melt are characterized by cation exchanges in which ^{M1}(Al, Fe^{3+}) substitute for ^{M2}(Mg, Fe^{2+}) coupled with replacement of Al with Si in the tetrahedral site. As a consequence, hedenbergite (Hd), enstatite (En), ferrosilite (Fs), jadeite (Jd) and tschermakitic components (∑Ts equals to the sum of Ca-, CaFe-, CaCr- and CaTi-Tschermak molecules) are preferentially incorporated in clinopyroxenes from the trachybasaltic lava (Fig. 2), whereas clinopyroxenes from the hybrid melt are enriched in diopside (Di). Despite these compositional variations, clinopyroxenes from Zone 1 and Zone 2 are invariably classified as diopside by the scheme of Morimoto (1988). The crystallization of Ti-Al-poor and Si-rich diopsidic crystals has been previously documented in the reaction coronas found at the interface between quartzite xenoliths and trachybasaltic lavas erupted during historic volcanic activity of Mt. Etna (Michaud and Clocchiatti, 1995).

To test whether clinopyroxenes from Zone 1 and Zone 2 were effectively in equilibrium with melts supplying chemical components to the growing crystals, the equilibrium model of Mollo et al. (2013b) was used. Clinopyroxene-melt pairs used for calculations are those reported in Table 1S, corresponding to the analyses of clinopyroxenes and glasses used for the calculation of Zone 1

and Zone 2 partition coefficients. The equilibrium is based on the difference (Δ) between diopside + hedenbergite (DiHd) contents measured in the analyzed crystals with those predicted for clinopyroxene via regression analysis of equilibrium clinopyroxene-melts pairs. Considering that ΔDiHd should equal to zero at thermodynamic equilibrium, the derived values (0.01–0.08) suggest near-equilibrium crystallization (Fig. 3a), plotting within 10% of the one-to-one line (cf. Mollo and Masotta, 2013). As a further test, we have used the equilibrium model of Putirka (2008) based on the Fe–Mg cation exchange reaction [$Kd_{Fe–Mg} = (Fe^{cpx} / Fe^{melt}) \times (Mg^{melt} / Mg^{cpx})$]. The measured values for $Kd_{Fe–Mg}$ (0.24–0.27; Fig. 3b) closely match with the equilibrium ranges of 0.27 ± 0.03 and 0.28 ± 0.08 indicated by Putirka et al. (2003) and Putirka (2008) respectively. These equilibrium clinopyroxene compositions were also used as input data for the *P*-H_2O-independent thermometer of Putirka et al. (1996) with uncertainty ±23 °C. Results show that Zone 1 clinopyroxenes formed from the trachybasaltic lava within a thermal range (~1,140-1,170 °C) consistent with the early saturation temperature of clinopyroxenes in Etnean magmas (Mollo et al., 2015b). Conversely, Zone 2 clinopyroxenes from the hybrid melt equilibrated at lower temperature conditions (~1,070-1,130 °C), suggesting crystallization when the ascending trachybasaltic magma encountered and interacted with the colder, shallower crustal basement.

4.3 Glass chemistry and melt hybridism

The residual melt from Zone 1 is chemically homogeneous basaltic trachyandesite (Fig. 4) with SiO_2 ≈ 51-52 wt.% and $Na_2O + K_2O$ ≈ 7-8 wt.%. Hundreds of microns from the interaction Zone 2, the interstitial glass in close contact with the quartz grains from Zone 3 is significantly enriched in SiO_2 (80-86 wt.%; Fig. 4), resembling the analyses of siliceous melts obtained by partial quartz dissolution (Watson, 1982). Conversely, the hybrid melt at the quartzite-lava interface from Zone 2 exhibits trachyandesitic to trachytic compositions (SiO_2 ≈ 56-68 wt.% and $Na_2O + K_2O$ ≈ 8-9 wt.%; Le Maitre et al., 2002) intermediate between those from Zone 1 and Zone 3 (Fig. 4). Major oxide analyses for SiO_2, Al_2O_3, FeO, MgO, and CaO almost plot on tie-lines between basaltic

trachyandesite and rhyolite end-members, indicative of a mixing process (Fig. 4). The contamination of the Etnean magma by progressive assimilation of a siliceous component is also evidenced by quantitative X-ray maps of the quartzite-lava interface (Fig. 5). The degree of hybridism between melts of markedly contrasting origin is better illustrated by Si-Al X-ray mapping overlays in which, among all major cations, silicon and aluminium show the greatest chemical variations (Fig. 6). From Zone 1 to Zone 3 via the hybrid melt of Zone 2, SiO_2 increases by ~69% relative, whereas Al_2O_3 decreases by ~75%. With respect to the original Al_2O_3/SiO_2 ratio (~0.31) of the Etnean magma (Table 3S), the final Al_2O_3/SiO_2 ratio (~0.15) of the hybrid melt decreases by ~50%, resembling the ^{T}Al-Si cation exchange observed for clinopyroxene (Fig. 2). Notably, the crystallization of clinopyroxene from the hybrid melt causes deviations from pure mixing trends. Depletions in MgO and CaO are observed in the hybrid melt next to the advancing crystal surface, whereas enrichments in Na_2O, K_2O, SrO, and BaO reflect the highly incompatible character of these elements within the clinopyroxene crystal lattice (Fig. 4). To estimate the degree of clinopyroxene crystallization from the hybrid melt, linear least-squares mass balance calculations are performed following the same strategy adopted by Barnes et al. (2002). Specifically, the simple mixing process between the basaltic trachyandesite from Zone 1 and siliceous component from Zone 3 (i.e., mixing end-members) is coupled with the crystallization of newly-formed clinopyroxenes from Zone 2. The trachyandesitic to trachytic compositions of the hybrid melt are fairly reproduced when the proportions of siliceous component and newly-formed clinopyroxenes are in the ranges of 8-30% and 6-18% respectively (Fig. 7). The goodness of fits is corroborated by the low sum of squares of residuals ($\sum r^2 \leq 0.23$).

4.4 Bulk-rock geochemistry

Bulk-rock compositions for the trachybasaltic lava (Table 3S) are very similar to those that typify recent eruptions. The Na_2O/K_2O ratio (~1.8) indicates that the lava can be defined as K-trachybasalt, in agreement with the shift from Na- to K-affinity of products erupted after the 1971

event (Viccaro and Cristofolini, 2008). Trace element concentrations show common features for historical Etnean basalts with negative anomalies in HFSE that reflect the imprint of slab-derived fluids in arc magmas originating from an OIB-type mantle source with relative enrichments in LILE and LREE (Corsaro and Metrich, 2016). The oxygen isotope ratio (6.1‰ $\delta^{18}O$; Table 3S) is also consistent with bulk-rock data (6.1-7.1‰ $\delta^{18}O$) obtained for previous lava flows (Viccaro and Cristofolini, 2008). Conversely, the quartzite bulk-rock composition (Table 3S) is similar to those previously reported for siliceous crustal xenoliths (SiO_2 > 90 wt.%) from 1982 to 1989 Etnean eruptions (Michaud, 1995) and from other volcanic settings (Harris and Chaumba, 2001; Fourie and Harris; 2011). The oxygen isotope composition of quartzite (12‰ $\delta^{18}O$; Table 3S) is higher than that measured for single quartz grains from siliceous crustal rocks (~8‰ $\delta^{18}O$), indicative of hydrothermal alteration phenomena (Harris and Chaumba, 2001; Fourie and Harris; 2011).

5. Discussion

5.1 Clinopyroxene-melt element partitioning

Zone 1 and Zone 2 partition coefficients discussed in this study are presented as Onuma diagrams (Onuma et al., 1968) in which elements are grouped by ionic charge for M1 and M2 clinopyroxene crystallographic sites and arranged from smallest to largest ionic radius (Shannon, 1976) within each group (Fig. 8). The graphical representation shows how strongly the partition coefficient is controlled by the properties of individual crystallographic sites. This excludes possible glass contamination effects during chemical analyses that, in turn, would yield irregular relationships among the partition coefficient, the valence of the element, and the ionic radius (Kennedy et al., 1993). As stated above, Zone 1 partition coefficients were derived using the compositions of clinopyroxene phenocrysts and those of the matrix glasses from the trachybasaltic lava. Conversely, Zone 2 partition coefficients were derived using the compositions of newly-formed clinopyroxenes and those of the hybrid glasses measured at the quartzite-magma interface. Both Zone 1 and Zone 2 partition coefficients of isovalent cations plotted against ionic radius lie on

parabola-like curves. However, Zone 2 partition coefficients show D_{TE}, D_{HFSE}, and D_{REE+Y} values lower that those measured for Zone 1 partition coefficients (Fig. 8). The opposite occurs for D_{LILE}, these divalent cations more favorably incorporated in newly-formed clinopyroxenes from Zone 2. Notably, Zone 1 partition coefficients closely match values derived for Etnean trachybasaltic magmas crystallized in the laboratory (Mollo et al., 2013c) and under natural conditions (Scarlato et al., 2014). Conversely, Zone 2 partition coefficients resemble those measured for more differentiated magmas with either alkaline or calcalkaline affinity, i.e. trachytes (Mahood and Stimac, 1990; Huang et al., 2006; Pappalardo et al., 2008), basaltic andesites (Zajacz and Halter, 2007), andesites (Luhr and Carmichael, 1980; Ewart and Griffin, 1994; Kleinn et al., 2000), and dacites (Bacon and Druitt, 1988).

Clinopyroxenes from both Zone 1 and Zone 2 show that LILE in M2 shift from mildly incompatible (e.g., $D_{Sr} < 0.9$) to highly incompatible (e.g., $D_{Ba} < 0.0009$; Fig. 8). REE+Y are incompatible within the crystal lattice but, from smallest to largest ionic radius, HREE (e.g., $D_{Yb} < 0.4$) are more easily accommodated in clinopyroxene relative to LREE (e.g., $D_{La} < 0.1$). Tetravalent cations from HFSE group are moderately incompatible in M1, showing $D_{Ti} \approx D_{Hf} < 0.7$ and $D_{Zr} < 0.2$ (Fig. 8). TE partition coefficients are either compatible (D_{Cr} and $D_{Sc} > 1.7$) or incompatible (D_{Cr} and $D_{Sc} < 1$) within clinopyroxenes from Zone 1 and Zone 2 respectively. Trace element partitioning of different valence cations onto M2 exhibits decoupled behavior characterized by increments of 2+ LILE cations (e.g., Sr) and decrements of 4+ HFSE cations (e.g., Hf). From Zone 1 to Zone 2 clinopyroxenes, the partitioning parabola shifts upward for divalent LILE cations on M2 (Fig. 8), whereas the opposite occurs for D_{TE}, D_{HFSE}, and D_{REE+Y}, paralleling the decreasing number of Al cations in the tetrahedral site (Lindstrom, 1976; Ray et al., 1983; Hart and Dunn, 1993; Forsythe et al., 1994; Lundstrom et al., 1994, 1998; Skulski et al., 1994; Blundy et al., 1998; Hill et al., 2000; Wood and Trigila, 2001; Bedard, 2014). The different incorporation of trace elements in clinopyroxenes from Zone 1 and Zone 2 is related to charge balance mechanisms (Blundy and Wood, 1994, 2003; Wood and Blundy, 1997; Lundstrom et al., 1998) primarily

controlled by ^{T}Al (Fig. 9). The entry of HFSE onto M1 in Zone 1 clinopyroxene is facilitated because the average charge on M1 increases with increasing ∑Ts (Fig. 2) due to replacement of Mg^{2+} by Fe^{3+} and Al^{3+} (Wood and Trigila, 2001; Marks et al., 2004). Similarly, the dependence of D_{REE+Y} on ^{T}Al is interpreted as the increasing probability of achieving charge-neutral local configurations (e.g., $REEMgSiAlO_6$) where REE+Y enter in a locally charge-balanced M2 site with increasing ^{T}Al (Blundy et al., 1998). Such configurations do not involve electrostatic work of substitution of the trace element (Wood and Blundy, 2001) and, therefore, the Onuma parabola shifts upward in Al-rich clinopyroxenes from Zone 1 (Fig. 8). Conversely, decreasing Al concentrations in clinopyroxenes from Zone 2 make local charge balancing on M2 difficult, such that Al-poor clinopyroxenes cannot easily accommodate REE+Y into their crystal lattices (Hill et al., 2000; Wood and Trigila, 2001). It has been widely documented that REE+Y replace Ca in M2 while charge balanced by Al replacing Si in tetrahedral site or Na replacing Ca in M2 (Gaetani and Grove, 1995; Blundy et al., 1998; Schosnig and Hoffer, 1998; Bennett et al., 2004; Marks et al., 2004; Francis and Minarik, 2008; Sun and Liang, 2012). This compensation mechanism applies well to Zone 1 clinopyroxenes (Fig. 2). In contrast, Zone 2 crystals are significantly depleted in ^{T}Al and Na greatly reducing the number of possible local charge-balanced configurations (cf. Wood and Blundy 2001). As a consequence, trivalent TE (Sc^{3+}, Cr^{3+}) decrease from Zone 1 to Zone 2 crystals (Fig. 9), due to a decreased net charge in M1 (Bedard, 2014) resulting from lower Fe^{3+} contents (Hill et al. 2000), whereas divalent LILE cations (Sr^{2+}, Pb^{2+}, Ba^{2+}) increase in the M2 site of Zone 2 clinopyroxenes (Fig. 9), due to the higher ^{M2}Ca in the more diopsidic crystals (cf. Michaud, 1995; Michaud and Clocchiatti, 1995).

5.2 Modeling trace element partitioning through the lattice strain theory

In Onuma diagrams, the parabolic trend of partition coefficients measured for an isovalent series of cations can be described quantitatively by the lattice strain model (Brice, 1975; Blundy and Wood, 1994; Wood and Blundy, 1997):

$$D_i = D_0 \exp\left(\frac{-4\pi E N_A \left(\frac{r_0}{2}(r_i - r_0)^2 + \frac{1}{3}(r_i - r_0)^3 \right)}{RT} \right) \quad (1)$$

where D_i and r_i are, respectively, the partition coefficient and ionic radius of the element *i* of interest, D_0 is the partition coefficient for the strain-free substitution, r_0 is the radius of a hypothetical cation that substitutes into the site with zero strain, *E* is the effective Young's modulus for the lattice site, N_A is Avogadro's number (6.022×10^{23} mol^{-1}), *R* is the universal gas constant (8.3145 J mol^{-1} K^{-1}), and *T* is the temperature (in Kelvin). To obtain reliable estimates and minimize the standard error, the lattice strain model requires the determination of partition coefficients for a large range of isovalent cations (Yao et al., 2012; Sun and Liang, 2013; Bedard, 2014). On this basis, r_0, D_0, and *E* have been determined for the partitioning of trivalent REE+Y, as these form the largest group of isovalent elements in the analytical dataset (Table 4S). Linear regression fits and their correlation coefficient (R^2) show a high dependence of r_0 ($R^2 = 0.94$), D_0 ($R^2 = 0.95$), and *E* ($R^2 = 0.94$) on ^{T}Al of Zone 1 and Zone 2 clinopyroxenes (Fig. 10a). D_0 increases due to the increasing probability of cations entering a locally charge-balanced site as the ^{T}Al increases (Wood and Blundy 2001). Conversely, r_0 and *E* decrease with increasing ^{T}Al (Fig. 10a), corroborating the inverse correlation between r_0 and ^{T}Al (Adam and Green, 2006; Tuff and Gibson, 2007), as well as the positive linear dependence of *E* on r_0 found for clinopyroxenes (Sun and Liang, 2012) and low-Ca pyroxenes (Yao et al., 2012).

If the melt composition has minor effects on D_{REE+Y}, the height of the partitioning parabola is expected to increase with increasing aluminum in the tetrahedral site and with decreasing temperature (Hill et al., 2000; Wood and Trigila 2001). However, the control of melt composition and structure on element partitioning cannot be excluded because the clinopyroxenes and melts result from a progressive mixing process between two compositionally distinct aluminosilicate liquids (Figs. 4, 5, and 6). Therefore, with respect to the uncontaminated trachybasaltic magma, the effect of ^{T}Al on the lattice strain parameters can be mediated by the increasingly silicic character of

the hybrid melt (Gaetani 2004). Data from mafic melts show diffuse increase of D_{REE+Y} with ^{T}Al, but data from felsic melts show less robust trends due to the influence of melt composition (Bedard, 2014). For clinopyroxenes with similar ^{T}Al contents, D_{REE+Y} can increase by up to an order of magnitude as a result of the dominant effect of melt structure (Qian et al., 2015). The degree of melt polymerization may affect the trace element partitioning when the number of non-bridging oxygens per tetrahedral cations (NBO/T) is lower than 0.49 (Gaetani 2004). However, over a broad range of melt compositions the influence of melt structure on D_{REE+Y} is more effective below the NBO/T threshold of 0.25 (Huang et al., 2006; Mollo et al., 2015). NBO/T values from this study range from 0.31 to 0.43 and, therefore, D_0 (R^2 = 84) is poorly correlated with the degree of melt polymerization (Fig. 10b). Notably, the effect of melt structure is usually insignificant on r_0 (R^2 = 81) and E (R^2 = 81) values (cf. Qian et al., 2015). On the one hand, it has been found that NBO/T is not a good predictor for the lattice strain model (Sun and Liang; 2012; Mollo et al., 2016). On the other hand, due to the similarity in ionic radius and charge, REE+Y are more likely to substitute for Ca in the melt relative to other divalent (Fe + Mg) and monovalent (Na + K) cations (Huang et al., 2006). When the influence of clinopyroxene chemistry is minimized, D_0 (at fixed temperature) strictly depends on the melt structure expressed as the ratio of molar Ca /(Na + K + Fe + Ca + Mg) where cations are given as percentages (Huang et al., 2006). Data from this study exhibit a weak correlation (R^2 = 86) between D_0 and Ca /(Na + K + Fe + Ca + Mg) of the melt, testifying to rival effects between the increase in the number of large structural sites critically important to accommodating trace element cations in the melt and the strong control of clinopyroxene chemistry on REE+Y partitioning (Mollo et al., 2016). It is noteworthy that a regular solution model for predicting the effect of melt structure on REE+Y partition coefficient has been derived only when the melt composition changes drastically from gabbroic to granitic (Schmidt et al., 2006).

In order to better define the effect of clinopyroxene composition on REE+Y (i.e., D_{La} and D_{Lu}) and HFSE (i.e., D_{Ti} and D_{Zr}) partitioning, the dataset from this study has been compared with values predicted by the models of Wood and Blundy (1997) and Hill et al. (2011) (Table 5S). These

thermodynamically-derived equations are based on the lattice strain parameters and allow for discrimination and quantification of the primary compositional effects on trace element partitioning. Wood and Blundy (1997) parameterized the predictive model for REE+Y as functions of pressure (*P*), temperature (*T*), *Mg*-number of the melt [*Mg#* = molar Mg/(Mg+Fe)] and ^{M1}Mg of clinopyroxene, also considering that ^{M2}Ca and ^{M1}Al affect REE+Y partitioning through their influence on r_0. The input values used are the entrapment pressure (100 MPa) of the quartzite xenoliths, the crystallization temperature of clinopyroxenes (1,140-1,170 °C and 1,070-1,130 °C for Zone 1 and Zone 2, respectively), and major element compositions of crystal and coexisting glass (Table 1S). The control of pressure on D_{REE+Y} and D_{Na} is practically negligible at shallow crustal depths (Blundy et al., 1995; Blundy and Wood, 2003; Bennett et al., 2004). Additionally, the low (< 2 wt.%) concentration of H_2O dissolved in the Etnean magmas residing at shallow pressure (Perinelli et al., 2016) has negligible effects on the activity of $REEMgAlSiO_6$ (Wood and Blundy, 2002).

D_{La} and D_{Lu} are well predicted by the lattice strain model (Fig. 11), yielding high correlation coefficients (R^2_{La} = 0.96 and R^2_{Lu} = 0.94) and low standard errors of estimate (SEE_{La} = 0.002 and SEE_{Lu} = 0.01). As D_{La} and D_{Lu} decrease from Zone 1 to Zone 2 clinopyroxenes (Fig. 11), the shape of REE+Y partitioning remains subparallel in the Onuma diagram (Fig. 8), suggesting preferential control of crystal chemistry rather than melt structure (Hill et al., 2000; Wood and Trigila 2001; Qian et al., 2015). Considering the intrinsic calibration error of the model, values of r_0 are also fairly reproduced by the expression (R^2 = 0.93 and SEE = 0.001) of Wood and Blundy (1997) based on ^{M1}Al and ^{M2}Ca, as well as by the more recent equation (R^2 = 0.94 and SEE = 0.001) of Sun and Liang (2012) based on ^{M1}Al and ^{M2}Mg. The shape of the partitioning parabola is determined by compositional variations from Zone 1 to Zone 2 clinopyroxenes in which lower ^{T}Al is accompanied by decreasing ^{M1}Al and increasing ^{M2}Mg and ^{M2}Ca during formation of Di-rich crystals (Fig. 2). Wood and Blundy (1997) modelled D_{REE+Y} as independent of ^{T}Al, assuming simple short-range order between REE+Y on M2 site and Al in T site in the $REEMgAlSiO_6$ molecule. Wood and

Trigila (2001) attempted to refit the lattice strain model by including ^{T}Al but no improvements were found. Additionally, the prediction ability of the model does not change by including the electrostatic work for local charge balance between REE+Y in M2 and adjacent ^{T}Al (Mollo et al., 2016). Looking at the test dataset used by Wood and Trigila (2001), it is apparent that values of ^{T}Al and ^{M1}Al decrease in concert with higher ^{M1}Mg and ^{M2}Mg contents, where ^{M1}Mg is the expression of the activity of $REEMgAlSiO_6$ clinopyroxene ($a^{cpx}_{REEMgAlSiO6} = X^{M2}_{REE} X^{M1}_{Mg}$ in mole fraction) and ^{T}Al is negatively correlated with ^{M2}Mg (Sun and Liang, 2012). This leads to the conclusion that simultaneous cation exchanges across the M1, M2 and T sites, such as those observed in this study, make the ^{T}Al term statistically unimportant for the original model of Wood and Blundy (1997). In other words, over a broad calibration dataset the dependence of D_{REE+Y} on ^{T}Al is obscured by other compositional effects (cf. Wood and Trigila, 2001), such as those related to ^{M2}Ca (Wood and Blundy, 2001), ^{M2}Mg (Sun and Liang, 2012), and ^{M1}Fe (Dygert et al., 2014).

For the case of HFSE, Hill et al. (2011) modelled D_{Ti} through a thermodynamic description for the crystal-melt exchange reaction and the energetics of the different charge-imbalanced configurations produced by insertion of a heterovalent cation. The authors derived expressions for *E* and r_0 of the M1 site as a function of pressure, temperature, and composition where D_{Ti} serves also as a proxy for the prediction of D_{Hf} and D_{Zr} (cf. Blundy and Wood, 2003). Fits of predicted against measured values (Fig. 11) provide good regression statistics for D_{Ti} (R^2_{Ti} = 0.96 and R^2_{Ti} = 0.94) and D_{Zr} (SEE_{Ti} = 0.96 and SEE_{Ti} = 0.94). Considering the electrostatic effect produced by insertion of a cation of different charge from the major cation (e.g., Ti^{4+} for Mg^{2+}) into the crystal lattice, the proportion of M1 sites charge-balanced by a tetravalent cation decreases (from 0.018 to 0.001) with increasing ^{M1}Mg from Zone1 to Zone 2 clinopyroxenes. As demonstrated by Wood and Blundy (2001), however, cations are also likely to be present in sites of unbalanced charge. The electrostatic work done in placing HFSE into a crystal site of the wrong charge from Zone 1 to Zone 2 clinopyroxenes can be quantified by the model of Hill et al. (2011). It is found that the proportion of M1 sites charge balanced by a trivalent cation decreases (from 0.031 to 0.017) with decreasing ^{M1}Al,

confirming that the average energy of HFSE substitution is effectively related to the concentrations of the different types of charged or uncharged sites in the clinopyroxene structure (cf. Wood and Blundy, 2001). Owing to charge balancing, the decrease of D_{Ti} is also positively correlated with D_{REE+Y} (Fig. 11), as the ^{T}Al/Si ratio of clinopyroxene decrease from Zone 1 to Zone 2 (Fig. 2). A similar relationship has been reported by Hack et al. (1994) and recently reappraised by global regression fits of Bedard (2014). Titanium much more readily enters the M1 site of $CaAl_2SiO_6$ (3+ charge on M1) than $CaMgSi_2O_6$ (2+ charge on M1). Consequently, D_{Ti} increases with increasing ^{T}Al during substitution of diopside with Tschermak molecules and replacement of divalent Mg with trivalent Fe and Al (Wood and Trigila, 2001). In contrast, the substitution of REE+Y onto M2 is facilitated for the molecule $REEMgAlSiO_6$ in which the charge on M1 does not increase with increasing ^{T}Al. Indeed, M2 is almost exclusively occupied by divalent Ca, Mg, and Fe, apart from minor amounts of monovalent Na. Thus, charge imbalances associated with the entry of trivalent REE+Y cations into M2 cause D_{REE+Y} to increase with ^{T}Al in concert with an increased ease of locally balancing the excess charge at M2 as the number of surrounding tetrahedral Al atoms increases (Hill et al., 2000).

When magma evolution is modelled by petrologists, the partition coefficients are frequently assumed to be constant during the entire evolution of magma owing to obvious oversimplifications that do not take into account the dependence of trace element partitioning on *P*, *T*, and *X*. Undoubtedly, as the physicochemical conditions of the natural system change, a variety of partition coefficient values contribute to determining the final compositions of the solid products. To illustrate the change of REE+Y partitioning during magma differentiation, MELTS (Ghiorso and Sack, 1995) thermodynamic simulations were performed using as initial melt composition the bulk-rock analysis of the trachybasaltic lava (Table 6S). The simulations started from the melt liquidus temperature (1,170 °C) assuming pressure (100 MPa), melt-H_2O content (1.5 wt.%), and oxygen fugacity (nickel-nickel oxide) comparable to those estimated for recent eruptions at Mt. Etna (Mollo et al., 2015b). The compositions of clinopyroxenes and coexisting melts recovered by MELTS code

were then used as input data for the lattice strain model of Wood and Blundy (1997). D_0 values predicted for the partitioning of REE+Y during magma differentiation are plotted against T and ^{T}Al, and compared with D_0 measured for Zone 1 and Zone 2 clinopyroxenes (Fig. 12). Notably, T and ^{T}Al influence strongly D_{REE+Y}, as well as the shape of the parabola in the Onuma diagram (Sun and Liang, 2012). Changing a single parameter at a time, it is found that D_0 increases with (i) decreasing T due to the positive entropy of fusion of silicate minerals (Wood and Blundy, 1997) and (ii) increasing ^{T}Al in response to local charge balance requirements (Hill et al., 2000). On this basis, the partitioning behaviour of REE+Y predicted along the evolutionary path of trachybasaltic magma is opposite to that measured during melt contamination by siliceous crustal material (Fig. 12). Over an almost identical temperature decrease of ~70 °C, two different scenarios are observed: (1) D_0 increases by ~32% during magma differentiation when ^{T}Al slightly decreases by ~17% and (2) D_0 decreases by ~19% during magma contamination when ^{T}Al drastically decreases by ~76%. Unravelling the combined effects of T and ^{T}Al is not a trivial task when the compositions of clinopyroxene and coexisting melt change systematically as a function of the intensive variables of the system. However, it is also true that much progress has been made in recent years (Yao et al., 2012; Sun and Liang, 2012, 2013; Dygert et al., 2014; Dygert and Liang, 2015; Qian et al., 2015). For example, Sun and Liang (2012) demonstrated that temperature and clinopyroxene composition may have either a competing effect or an enhancing effect on D_{REE+Y} during adiabatic mantle melting, depending on how ^{T}Al in clinopyroxene varies as a function of T. Furthermore, during assimilation of olivine xenocrysts (or peridotite xenoliths) and simultaneous crystallization of clinopyroxene, Qian et al. (2015) showed that the behaviour of D_{REE+Y} and D_{HFSE} diverges with the decreasing temperature, due to inverse covariation between Al and Mg favouring Tschermak molecules. Turning to the case of magmatic evolution at Mt. Etna, the rate of temperature decrease is the dominant factor controlling D_0 in scenario (1) when changes in ^{T}Al are relatively small in clinopyroxenes formed during magma differentiation (Fig. 12). Conversely, in scenario (2), REE+Y become more incompatible within the clinopyroxene crystal lattice (Fig. 12), due to the marked ^{T}Al

deficiency that virtually overcomes the enhancing effect of temperature decrease. Extrapolation of this finding to larger spatial and temporal scales leads to the conclusion that assimilation of siliceous crustal components may favor the formation of diopsidic clinopyroxene-rich layers. However, changes of clinopyroxene chemistry due to crustal contamination have dramatic effects on the magnitude of trace element partitioning due to limited cation incorporation into the newly-formed crystals.

Following De Paolo (1981), partition coefficients for Ce and Y from scenario (1) and scenario (2) were used to model the differentiation process driven by either fractional crystallization (FC) or assimilation and fractional crystallization (AFC). These simple, but different, models may help to elucidate the control of clinopyroxene on the final trace element content of magma. Stepwise calculations were performed changing the partition coefficient at each step of fractionation as a function of temperature and clinopyroxene chemistry. Starting from the original bulk-rock composition of the trachybasaltic magma, four different degrees of clinopyroxene fractionation (i.e., 5%, 10%, 15%, and 20%) were considered over the restricted temperature range of ~70 °C. The quartzite bulk-rock was assumed as the assimilant; the assimilation rate relative to fractional crystallization rate was set to 0.1. When both FC and AFC processes are modeled by D_{Ce} and D_{Y} from scenario (1), two similar trajectories are derived for the temperature-dependent partition coefficients (Fig. 13a). In contrast, Ce and Y from scenario (2) show substantial enrichments in the contaminated magma, due to the formation of diopside-rich clinopyroxenes that are highly depleted in aluminium and less inclined to incorporate REE+Y (Fig. 13a). This causes melt hybridization and subsequent clinopyroxene crystallization to produce REE+Y enrichments that cannot be modeled by simple variation of the partition coefficient along the thermal path of the system. For the sake of completeness, the clinopyroxene and coexisting melt compositions recovered by MELTS code (Table 6S) were adopted to estimate the partition coefficients of HFSE through the thermodynamic expression of Hill et al. (2011). Using the same stepwise calculations described above, the evolution of magma is modelled for D_{Ti} and D_{Zr} as a function of temperature and mineral

chemistry. Similarly to what is observed for D_{Ce} and D_Y from scenario (2), the weak incorporation of Ti and Zr into diopside-rich clinopyroxenes of hybrid origin results in an AFC trajectory much steeper than that found for the temperature-dependent partition coefficients, showing considerable HFSE enrichments in the contaminated magma relative to FC and AFC processes from scenario (1) (Fig. 13b).

6. Concluding remarks

The petrological consequence of Etnean magma contamination by siliceous continental crust is the formation of a hybrid melt favoring crystallization of clinopyroxenes that are compositionally distinct from those found in the uncontaminated magma. Diopside-rich clinopyroxenes from the hybrid melt result from cation exchanges in which $^{M1}(Al, Fe^{3+})$ substitute for $^{M2}(Mg, Fe^{2+})$ coupled with replacement of Si with Al in the tetrahedral site. The incorporation of trace elements in the crystal lattice is related to charge balance mechanisms primarily controlled by ^{T}Al. Specifically, hybrid clinopyroxenes depleted in Al cannot easily accommodate REE+Y in M2 as the number of local charge-balanced configurations decreases. Through the lattice strain theory, it is also found that simultaneous cation exchanges across the M1, M2, and T sites have profound effects on the partitioning of REE+Y and HFSE that, in turn, are weakly dependent on temperature and melt composition. Consequently, the behavior of REE+Y and HFSE observed during melt hybridization diverges significantly from that measured along the thermal path of the magma, leading to unexpected trace element enrichments due to low cation incorporations into the crystal lattice of hybrid clinopyroxenes.

Acknowledgments

We gratefully acknowledge Q. Qian and an anonymous reviewer for their useful and constructive criticism. The authors thank also A. Kerr for his valuable editorial guidance. This research was

supported by MIUR, Premiale project — NoRth: New hORizons of the Technology applied to experimental researches and geophysical and volcanological monitoring.

References

Adam, J., Green, T., 2006. Trace element partitioning between mica- and amphibole-bearing garnet lherzolite and hydrous basanitic melt: 1. Experimental results and the investigation of controls on partitioning behaviour. Contributions to Mineralogy and Petrology 152, 1–17.

Applegarth, L.J., Tuffen, H., James, M.R., Pinkerton, H., Cashman, K.V., 2013. Direct observations of degassing-induced crystallization in basalts. Geology 41, 243–246.

Armienti, P., Perinelli, P., Putirka, K., 2013. A new model to estimate deep-level magma ascent rates, with applications to Mt. Etna (Sicily, Italy). Journal of Petrology. http://dx.doi.org/10.1093/petrology/egs085.

Bacon, C.R., Druitt, T.H., 1988. Compositional evolution of the zoned calcalkaline magma chamber of Mount Mazama, Crater Lake, Oregon. Contributions to Mineralogy and Petrology 98, 224-256.

Barnes, C.G., Yoshinobu, A.S., Prestvik, T., Nordgulen, a., Karlsson, H.R., Sundvoll, B., 2002. Mafic magma intraplating: anatexis and hybridization in arc crust, Bindal Batholith, Norway. Journal of Petrology 43, 2171–2190.

Bédard, J.H., 2014. Parameterizations of calcic pyroxene-melt trace element partition coefficients. Geochem. Geophys. Geosyst. 15, 303-336.

Behncke, B., Branca, S., Corsaro, R.A., De Beni, E., Miraglia, L., Proietti, P., 2014. The 2011–2012 summit activity of Mount Etna: birth, growth and products of the new SE crater. J. Volcanol. Geotherm. Res. 270, 10–21.

Bennett, S.L., Blundy, J., Elliott, T., 2004. The effect of sodium and titanium on crystal–melt partitioning of trace elements. Geochimica et Cosmochimica Acta 68, 2335–2347. http://dx.doi.org/10.1016/J.Gca.2003.11.006.

Bergantz, G.W., Dawes, R. 1994. In Magmatic Systems; Ryan, M. P.; Aspects of magma generation and ascent in continental lithosphere; CA: Academic Press: San Diego, California, 1994, pp 291-317.

Blundy, J., Wood, B., 1994. Prediction of crystal–melt partition-coefficients from elastic moduli. Nature 372 (6505), 452–454. http://dx.doi.org/10.1038/372452a0.

Blundy, J., Wood, B., 2003. Partitioning of trace elements between crystals and melts. Earth and Planetary Science Letters 210 (3–4), 383–397. http://dx.doi.org/10.1016/S0012-821x(03)00129–8.

Blundy, J.D., Falloon, T.J., Wood, B.J., Dalton, J.A., 1995. Sodium partitioning between clinopyroxene and silicate melts. Journal of Geophysical Research 100, 15501–15516.

Blundy, J.D., Robinson, J.A.C., Wood, B.J., 1998. Heavy REE are compatible in clinopyroxene on the spinel lherzolite solidus. Earth and Planetary Science Letters 160 (3–4), 493–504. http://dx.doi.org/10.1016/S0012-821x(98)00106-X.

Branca, S., Coltelli, M., Groppelli, G., Lentini, F., 2011. Geological map of Etna volcano, 1: 50,000 scale. Italian Journal of Geosciences 130, 265–291

Brice, J.C., 1975. Some thermodynamic aspects of the growth of strained crystals. J Cryst Growth 28:249–253

Clocchiatti, R., Condomines, M., Guenot, N., Tanguy, J.C., 2004. Magma changes at Mount Etna: the 2001 and 2002–2003 eruptions. Earth and Planetary Science Letters 226, 397–414.

Corsaro, R.A., Métrich, N., 2009. Chemical heterogeneity of Mt. Etna magmas in the last 15 ka. Inferences on their mantle sources. Lithos 252–253, 123–134.

Corsaro, R.A., Di Renzo, V., Distefano, S., Miraglia, L., Civetta, L., 2013. Relationship be- tween petrologic processes in the plumbing system of Mt. Etna and the dynamics of the eastern flank from 1995 to 2005. J. Volcanol. Geotherm. Res. 251, 75–89.

Corsaro, R.A., Miraglia, L., 2014. The transition from summit to flank activity at Mt. Etna, Sicily (Italy): inferences from the petrology of products erupted in 2007–2009. Journal of Volcanology and Geothermal Research 275, 51–60.

Costa, F., Dungan, M., 2005. Short time scales of magmatic assimilation from diffusion modeling of multiple elements in olivine. Geology 2005, 33, 837-840.

Cribb, J.W., Barton, M., 1996. Geochemical effects of decoupled fractional crystallization and crustal assimilation. Lithos 37, 293 – 307.

De Paolo, D.J., 1981. Trace element and isotopic effects of com- bined wallrock assimilation and fractional crystallization. Earth Planet. Sci. Lett. 53, 189–202.

Dungan, M.A., Davidson, J.P., 2004, Partial assimilative recycling of the mafic plutonic roots of arc volcanoes: An example from the Chilean Andes. Geology 32, 773–776.

Dygert N. and Liang Y. (2015) Temperature and cooling rates recorded in REE in coexisting pyroxenes in ophiolitic and abyssal peridotites. Earth Planet. Sci. Lett. 420, 151–161.

Dygert, N., Liang, Y., Sun, C.G., Hess, P., 2014. An experimental study of trace element partitioning between augite and Fe-rich basalts. Geochim. Cosmochim. Acta 132, 170–186.

Erdmann, S., London, D., Morgan VI, G.B., Clarke, D.B., 2007. Contamination of granitic magma by metasedimentary country-rock material: an experimental study. Canadian Mineralogist 45, 43–61.

Ewart, A., Griffin, W.L., 1994. Application of proton-microprobe data to trace-element partitioning in volcanic-rocks. Chemical Geology 117, 251-284.

Ferlito, C., Viccaro, M., Cristofolini, R., 2008. Volatile-induced magma differentiation in the plumbing system of Mt. Etna volcano (Italy): evidence from glass in tephra of the 2001 eruption. Bull. Volcanol. 70, 455–473.

Ferlito, C., Viccaro, M., Nicotra, E., Cristofolini, R. 2011. Regimes of magma recharge on the eruptive behaviour during the period 2001–2005 at Mt. Etna volcano. Bull Volcanol 74, 533–543 http://dx.doi.org/10.1007/s00445-011-0537-1

Forsythe, L.M., Nielsen, R.L., Fisk, M.R. 1994. High-field strength element partitioning between pyroxene and basaltic to dacitic magmas. Chem Geol 117, 107–125.

Fourie, D.S., Harris, C., 2011. O-isotope study of the Bushveld Complex Granites and Granophyres: constraints on source composition, and assimilation. Journal of Petrology 52, 2221-2242.

Francis, D., Minarik, W. 2008. Aluminum-dependent trace element partitioning in clinopyroxene. ContribMineral Petrol 156, 439–451. http://dx.doi.org/10.1007/s00410-008-0295-z

Gaetani, G.A., Grove, T.L., 1995. Partitioning of rare-earth elements between clinopyroxene and silicate melt–crystal-chemical controls. Geochim. Cosmochim. Acta 59, 1951–1962. http://dx.doi.org/10.1016/0016–7037(95)00119–0.

Gaetani, G.A., 2004. The influence of melt structure on trace element partitioning near the peridotite solidus. Contributions to Mineralogy and Petrology 147, 511–527. http://dx.doi.org/10.1007/S00410–004-0575-1.

Gamble, J.A., Wood, C.P., Price, R.C., Smith, I.E.M., Stewart, R.B., Waight, T., 1999. A fifty year perspective of magmatic evolution on Ruapehu Volcano, New Zealand: verification of open system behaviour in an arc volcano. Earth Planet. Sci. Lett. 170, 301-314.

Ghiorso, M.S., Sack, R.O., 1995. Chemical mass-transfer in magmatic processes IV. A revised and internally consistent thermodynamic model for the interpolation and extrapola- tion of liquid–solid equilibria in magmatic systems at elevated-temperatures and pressures. Contrib. Mineral. Petrol. 119, 197–212.

Giacomoni, P.P., Ferlito, C., Coltorti, M., Bonadiman, C., Lanzafame, G., 2014. Plagioclase as archive of magma ascent dynamics on “open conduit" volcanoes: the 2001–2006 eruptive period at Mount Etna. Earth-Science Reviews 138, 371–393.

Grove, T.L., Kinzler, R.J., Baker, M.B., Donnelly-Nolan, J.M., Lesher, C.E., 1988. Assimilation of granite by basaltic magma at Burnt Lava flow, Medicine Lake volcano, northern California. Contr. Min. Petr. 99, 320-343.

Hack, P.J., Nielsen, R.J., and Johnston, A.D., 1994. Experimentally determined rare-earth element and Y partitioning behavior between clinopyroxene and basaltic liquids at pressure up to 20 kbar. Chem. Geol. 117, 89–105.

Harris, C., Chaumba, J.B., 2001. Crustal contamination and fluid-rock interaction during the formation of the Platreef, Northern Limb of the Bushveld Complex, South Africa. Journal of Petrology 42, 1321–1347.

Hart, S.R., Dunn, T., 1993. Experimental Cpx melt partitioning of 24 trace-elements. Contributions to Mineralogy and Petrology 113, 1–8. http://dx.doi.org/10.1007/Bf00320827.

Heap, M.J., Mollo, S., Vinciguerra, S., Lavallée, Y., Hessm K.-U., Dingwell, D.B., Baud, P., Iezzi, G., 2013. Thermal weakening of the carbonate basement under Mt. Etna volcano (Italy): implications for volcano instability. J Volcanol Geotherm Res 250, 42–60. http://dx.doi.org/10.1016/j.jvolgeores.2012.10.004

Hildreth, W., Moorbath, S., 1988. Crustal contributions to arc magmatism in the Andes of Central Chile. Contr. Mineral. Petrol. 98, 455-489.

Hill, E., Wood, B.J., Blundy, J.D., 2000. The effect of Ca-Tschermaks component on trace element partitioning between clinopyroxene and silicate melt. Lithos 53, 203–215. http://dx.doi.org/10.1016/S0024–4937(00)00025–6.

Hill, E., Blundy, J.D., Wood, B.J., 2011. Clinopyroxene-melt trace element partitioning and the development of a predictive model for HFSE and Sc. Contrib Mineral Petr 161, 423–438. http://dx.doi.org/10.1007/s00410-010-0540-0.

Huang, F., Lundstrom, C.C., McDonough, W.F., 2006. Effect of melt structure on trace element partitioning between clinopyroxene and silicic, alkaline, aluminous melts. American Mineralogist 91, 1385–1400. http://dx.doi.org/10.2138/Am.2006.1909.

Huppert, H.E., Sparks, R.S.J., 1985. Cooling and contamination of mafic and ultramafic magmas during ascent through continental crust. Earth Planet. Sci. Lett. 74, 37–386.

Huppert, H.E., Sparks, R.S.J., 1988a. The generation of granitic magmas by intrusion of basalt into continental crust. J. Petrol. 29, 599–624.

Iezzi, G., Mollo, S., Torresi, G., Ventura, G., Cavallo, A., Scarlato, P. 2011. Experimental solidification of an andesitic melt by cooling. Chem Geol 283, 261–273. 10.1016/j.chemgeo.2011.01.024.

Iezzi, G., Mollo, S., Shaini, E., Cavallo, A., Scarlato, P., 2014. The cooling kinetics of plagioclase revealed by electron microprobe mapping. American Mineralogist 99, 898-907, http://dx.doi.org/10.2138/am.2014.4626.

Kahl, M., Chakraborty, S., Pompilio, M., Costa, F., 2015. Constraints on the nature and evolution of the magma plumbing system of Mt. Etna Volcano (1991–2008) from a combined thermodynamic and kinetic modelling of the compositional record of minerals. J. Petrol. 56, 2025-2068.

Kennedy, A.K., Lofgren, G.E., Wasserburg, G.J., 1993. An experimental study of trace element partitioning between olivine, orthopyroxene and melt in chondrules: equilibrium values and kinetic effects. Earth and Planetary Science Letters 115, 177–195. http://dx.doi.org/10.1016/0012-821X(93)90221-T.

Kerr, A.C., Kempton, P.D., Thompson, R.N., 1995. Crustal assimilation during turbulent magma ascent (ATA): new isotopic evidence from the Mull Tertiary lava succession, N.W. Scotland. Contrib. Mineral. Petrol. 119, 142–154.

Klein, M., Stosch, H-G., Seck, H.A., Shimizu, N., 2000. Experimental partitioning of high field strength and rare earth elements between clinopyroxene and garnet in andesitic to tonalitic systems. Geochim. Cosmochim. Acta. 64, 99–115.

Lanzafame, G., Mollo, S., Iezzi, G., Ferlito, C., Ventura, G., 2013. Unraveling the solidification path of a pahoehoe “cicirara” lava from Mount Etna volcano. Bulletin of Volcanology 75, 703-719. http://dx.doi.org/10.1007/S00445–013-0703-8.

Le Maitre, R.W., Streckeisen, A., Zanettin, B., Le Bas, M.J., Bonin, B., Bateman, P., Bellieni, G., Dudek, A., Efremova, S., Keller, J., Lamere, J., Sabine, P.A., Schmid, R., Sorensen, H., Woolley,

A.R., 2002. Igneous Rocks: A Classification and Glossary of Terms, Recommendations of the International Union of Geological Sciences, Subcommission of the Systematics of Igneous Rocks. Cambridge University Press, Cambridge.

Lindstrom, D.J., 1976. Experimental study of the partitioning of the transition metals between clinopyroxene and coexisting silicate liquids. Dissertation, University of Oregon, Corvallis, Oregon.

Lindsley, D.H., 1980. Phase equilibria of pyroxenes at pressure >1 atmosphere. In: Prewitt-Charles, T. (Ed.), Pyroxenes. Reviews in Mineralogy, vol 7. Mineralogical Society of America, Washington, DC, United States, pp. 289–307.

Luhr, J.F., Carmichael, I.S.E., 1980. The Colima volcanic complex, Mexico: I. Post-caldera andesites from Volcan Colima. Contrib. Mineral. Petrol. 71, 343–372.

Lundstrom, C.C., Shaw, H.F., Ryerson, F.J., Phinney, D.L., Gill, J.B., Williams, Q., 1994. Compositional controls on the partitioning of U, Th, Ba, Pb, Sr and Zr between clinopyroxene and haplobasaltic melts — implications for uranium series disequilibria in basalts. Earth and Planetary Science Letters 128, 407–423. http://dx.doi.org/10.1016/0012-821X(94)90159-7.

Lundstrom, C.C., Shaw, H.F., Ryerson, F.J., Williams, Q., Gill, J., 1998. Crystal chemical control of clinopyroxene–melt partitioning in the Di–Ab–An system: implications for elemental fractionations in the depleted mantle. Geochimica et Cosmochimica Acta 62, 2849–2862. http://dx.doi.org/10.1016/S0016–7037(98)00197–5.

Mahood, G., Stimac, J., 1990. Trace-element partitioning in pantellerites and trachytes. Geochimica et Cosmochimica Acta 54, 2257–2276.

Marks, M., Halama, R., Wenzel, T., Markl, G., 2004. Trace element variations in clinopyroxene and amphibole from alkaline to peralkaline syenites and granites: implications for mineral–melt trace-element partitioning. Chemical Geology 211, 185–215. http://dx.doi.org/10.1016/J.Chemgeo.2004.06.032.

Métrich, N., Allard, P., Spilliaert, N., Andronico, D., Burton, M., 2004. 2001 Flank eruption of the alkali- and volatile-rich primitive basalt responsible for Mount Etna's evolution in the last three decades. Earth and Planetary Science Letters 228, 1–17.

Michaud, V., Clocchiatti, R., 1995. Pyroxene features in crustal xenoliths from Etna: primary nature and elemental exchanges with magma. Acta Vulcanologica 5, 105-116.

Michaud, V., 1995. Crustal xenoliths in recent hawaiites from Mount Etna, Italy—evidence for alkali exchanges during magma-wall rock interaction. Chem Geology 122, 21–42.

Mollo, S., Masotta, M., 2014. Optimizing pre-eruptive temperature estimates in thermally and chemically zoned magma chamber. Chemical Geology 368, 97-103. 10.1016/j.chemgeo.2014.01.007.

Mollo, S., Vona, A., 2014. The geochemical evolution of clinopyroxene in the Roman Province: a window on decarbonation from wall-rocks to magma. Lithos 192–195, 1–7. http://dx.doi.org/10.1016/j.lithos.2014.01.009.

Mollo, S., Scarlato, P., Freda, C., Gaeta, M., 2011. Basalt-crust interaction processes: insights from experimental petrology, pp. 33-61, in West, J.P., eds., Basalt: Types, Petrology and Uses: New York, Nova Science Publishers, pp. 189. ISBN: 9781612096353.

Mollo, S., Heap, M.J., Iezzi, G., Hess, K.-U., Scarlato, P., Dingwell, D.B., 2012a. Volcanic edifice weakening via decarbonation: a self-limiting process?. Geophysical Research Letters 39, L15307. doi:10.1029/2012GL052613.

Mollo, S., Iezzi, G., Ventura, G., Cavallo, A., Scarlato, P., 2012b. Heterogeneous nucleation mechanisms and formation of metastable phase assemblages induced by different crystalline seeds in a rapidly cooled andesitic melt. Journal of Non-Crystalline Solids 358, 1624-1628. doi:10.1016/j.jnoncrysol.2012.04.010.

Mollo, S., Scarlato, P., Lanzafame, G., Ferlito, C., 2013a. Deciphering lava flow post-eruption differentiation processes by means of geochemical and isotopic variations: A case study from Mt. Etna volcano. Lithos 162-163, 115-127. http://dx.doi.org/10.1016/j.lithos.2012.12.020.

Mollo, S., Putirka, K., Misiti, V., Soligo, M., Scarlato, P., 2013b. A new test for equilibrium based on clinopyroxene-melt pairs: Clues on the solidification temperatures of Etnean alkaline melts at post-eruptive conditions. Chemical Geology 352, 92-100. doi: 10.1016/j.chemgeo.2013.05.026.

Mollo, S., Blundy, J., Scarlato, P., Iezzi, G., Langone, A., 2013c. The partitioning of trace elements between clinopyroxene and trachybasaltic melt during rapid cooling and crystal growth. Contributions to Mineralogy and Petrology 166, 1633-1654. doi: 10.1007/s00410-013-0946-6. Mollo et al., 2015

Mollo, S., Giacomoni, P.P., Andronico, D., Scarlato, P., 2015a. Clinopyroxene and titanomagnetite cation redistributions at Mt. Etna volcano (Sicily, Italy): Footprints of the final solidification history of lava fountains and lava flows. Chemical Geology 406, 45-54. http://dx.doi.org/10.1016/j.chemgeo.2015.04.017.

Mollo, S., Giacomoni, P.P., Coltorti, M., Ferlito, C., Iezzi, G., Scarlato, P., 2015b. Reconstruction of magmatic variables governing recent Etnean eruptions: constraints from mineral chemistry and P-T-fO2-H2O modelling. Lithos 212-215, 311-320. 10.1016/j.lithos.2014.11.020.

Mollo, S., Forni, F., Bachmann, O., Blundy, J. D., De Astis, G., Scarlato, P., 2016. Trace element partitioning between clinopyroxene and trachy-phonolitic melts: A case study from the Campanian ignimbrite (Campi Flegrei, Italy). Lithos 252–253, 160–172. doi:10.1016/j.lithos.2016.02.024.

Morimoto, N., 1988. Nomenclature of pyroxenes. Mineralogy and Petrology 39, 55–76. http://dx.doi.org/10.1007/BF01226262.

Onuma, N., Higuchi, H., Wakita, H., Nagasawa, H., 1968. Trace element partition between tw pyroxenes and host lava. Earth and Planetary Science Letters 5, 47-51. http://dx.doi.org/10.1016/S0012-821x(68)80010-X

Pappalardo, L., Ottolini, L., Mastrolorenzo, G., 2008. The Campanian Ignimbrite (southern Italy) geochemical zoning: insight on the generation of a super-eruption from catastrophic differentiation and fast withdrawal. Contributions to Mineralogy and Petrology 156, 1–26. http://dx.doi.org/10.1007/S00410–007-0270-0.

Perinelli, C., Mollo, S., Gaeta, M., De Cristofaro, S.P., Palladino, D.M., Armienti, P., Scarlato, P., Putirka, K.D., 2016. An improved clinopyroxene-based hygrometer for Etnean magmas and implications for eruption triggering mechanisms. American Mineralogist 101, 2774–2777. doi: 10.2138/am-2016-5916.

Pupier, E., Duchene, S., Toplis, M.J., 2008. Experimental quantification of plagioclase crystal size distribution during cooling of basaltic liquid. Contrib. Mineral. Petrol. 155, 555–570.

Putirka, K., Johnson, M., Kinzler, R., Longhi, J., Walker, D., 1996. Thermobarometry of mafic igneous rocks based on clinopyroxene-liquid equilibria, 0–30 kbar. Contributions to Mineralogy and Petrology 123, 92–108. http://dx.doi.org/10.1007/S004100050145.

Putirka, K., Ryerson, F.J., Mikaelian, H., 2003. New igneous thermobarometers for mafic and evolved lava compositions, based on clinopyroxene + liquid equilibria. American Mineralogist 88, 1542–1554.

Putirka, K., (2008) Thermometers and barometers for volcanic systems. In: Putirka K, Tepley F (eds) Minerals, inclusions and volcanic processes, vol 69, Reviews in mineralogy and geochemistry. Mineralogical Society of America, Chantilly, VA, USA, pp. 61–120.

Qian, Q., Hermann, J., Wang, Y., Guo, J., Liu, F., Wang, L., 2015. Variations of clinopyroxene/melt element partitioning during assimilation of olivine/peridotite by low-Mg diorite magma. Chemical Geology 419, 36-54.

Ray, G.L., Shimizu, N., Hart, S.R., 1983. An ion microprobe study of the partitioning of trace-elements between clinopyroxene and liquid in the system diopside-albite–anorthite. Geochimica et Cosmochimica Acta 47, 2131–2140. http://dx.doi.org/10.1016/0016–7037(83)90038–8.

Reiners, P.W., Nelson, B.K., Ghiorso, M.S., 1995. Assimilation of felsic crust by basaltic magma: thermal limits and extents of crustal contamination of mantle-derived magmas. Geology 23, 563–566.

Scarlato, P., Mollo, S., Blundy, J.D., Iezzi, G., Tiepolo, M., 2014. The role of natural solidification paths on REE partitioning between clinopyroxene and melt. Bulletin of Volcanology 76, 810. http://dx.doi.org/10.1007/S00445–014-0810-1.

Schiavi, F., Walte, N., Keppler, H., 2009. First in situ observation of crystallization processes in a basaltic–andesitic melt with the moissanite cell. Gelogy 37, 963–966.

Schmidt, M.W., Connolly, J.A.D., Gunther, D., Bogaerts, M., 2006. Element partitioning: the role of melt structure and composition. Science 312, 1646–1650

Schosnig, M., Hoffer, E., 1998. Compositional dependence of REE partitioning between diopside and melt at 1 atmosphere. Contrib. Mineral. Petrol. 133, 205–216.

Shannon, R.D., 1976. Revised effective ionic-radii and systematic studies of interatomic distances in halides and chalcogenides. Acta Crystallographica. Section A 32, 751–767. http://dx.doi.org/10.1107/S0567739476001551.

Skulski, T., Minarik, W., Watson, E.B., 1994. High-pressure experimental trace-element partitioning between clinopyroxene and basaltic melts. Chemical Geology 117, 127–147. http://dx.doi.org/10.1016/0009–2541(94)90125–2.

Spilliaert, N., Allard, P., Metrich, N., Sobolev, A.V., 2006. Melt inclusion record of the conditions of ascent, degassing, and extrusion of volatile-rich alkali basalt feeding the powerful 2002 flank eruption of Mount Etna (Italy). J. Geophys. Res. 111, B04203.

Sun, C.G., Liang, Y., 2012. Distribution of REE between clinopyroxene and basaltic melt along a mantle adiabat: effects of major element composition, water, and temperature. Contributions to Mineralogy and Petrology 163, 807–823. http://dx.doi.org/10.1007/S00410–011-0700-X.

Sun, C.G., Liang, Y., 2013. The importance of crystal chemistry on REE partitioning between mantle minerals (garnet, clinopyroxene, orthopyroxene, and olivine) and basaltic melts. Chemical Geology 358, 23–36. http://dx.doi.org/10.1016/J.Chemgeo.2013.08.045.

Tanguy, J.C., Condomines, M., Kieffer, G., 1997. Evolution of the Mount Etna magma: constraints on the present feeding system and eruptive mechanism. J. Volcanol. Geotherm. Res. 75, 221–250.

Tuff, J., Gibson, S.A., 2007. Trace-element partitioning between garnet, clinopyroxene and Fe-rich picritic melts at 3 to 7 GPa. Contributions to Mineralogy and Petrology 153, 369–387. http://dx.doi.org/10.1007/S00410–006-0152-X.

Vetere, F., Mollo, S., Giacomoni, P.P., Iezzi, G., Coltorti, M., Ferlito, C., Holtz, F., Perugini, D., Scarlato, P., 2015. Experimental constraints on the origin of pahoehoe "cicirara" lavas at Mt. Etna Volcano (Sicily, Italy). Bulletin of Volcanology 77, 44. doi: 10.1007/s00445-015-0931-1.

Viccaro, M., Cristofolini, R., 2008. Nature of mantle heterogeneity and its role in the short-term geochemical and volcanological evolution of Mt. Etna (Italy). Lithos 105, 272–288.

Viccaro, M., Calcagno, R., Garozzo, I., Giuffrida, M., Nicotra, E., 2015. Continuous magma recharge at Mt. Etna during the 2011–2013 controls the style of volcanic activity and compositions of erupted lavas. Min. Petrol. 109, 67–83, doi:10.1007/s00710-014-0352-4.

Watson, E.B., 1982. Basalt contamination by continental-crust: some experiments and models. Contributions to Mineralogy and Petrology 80, 73–87.

Wood, B.J., Blundy, J.D., 1997. A predictive model for rare earth element partitioning between clinopyroxene and anhydrous silicate melt. Contributions to Mineralogy and Petrology 129, 166–181. http://dx.doi.org/10.1007/S004100050330.

Wood, B.J., Blundy, J.D., 2001. The effect of cation charge on crystal–melt partitioning of trace elements. Earth and Planetary Science Letters 188, 59–71. http://dx.doi.org/10.1016/S0012-821x(01)00294–1.

Wood, B.J., Blundy, J.D., 2002. The effect of H_2O on crystal-melt partitioning of trace elements. Geochim. Cosmochim. Acta 66, 3647– 3656.

Wood, B.J., Trigila, R., 2001. Experimental determination of aluminous clinopyroxene–melt partition coefficients for potassic liquids, with application to the evolution of the Roman province potassic magmas. Chemical Geology 172, 213–223. http://dx.doi.org/10.1016/S0009–2541(00)00259-X.

Yao, L.J., Sun, C.G., Liang, Y., 2012. A parameterized model for REE distribution between low-Ca pyroxene and basaltic melts with applications to REE partitioning in low-Ca pyroxene along a mantle adiabat and during pyroxenite-derived melt and peridotite interaction. Contributions to Mineralogy and Petrology 164, 261–280. http://dx.doi.org/10.1007/S00410–012-0737-5.

Zajacz, Z., Halter, W., 2007. LA-ICPMS analyses of silicate melt inclusions in co-precipitated minerals: Quantification, data analysis and mineral/melt partitioning. Geochimica et Cosmochimica Acta 71, 1021-1040.

Figure captions

Fig. 1. Quartzite xenolith enclosed in a thin trachybasaltic lava envelope (a). Optical photomicrograph of the trachybasaltic lava (Zone 1), the hybrid melt resulting as a boundary layer between lava and quartzite (Zone 2), and the partially melted quartzite (Zone 3) (b). SEM photomicrograph in backscattered imaging mode of Zone 1, Zone 2, and Zone 3 (c). Detailed SEM photomicrograph of Zone 2 and Zone 3 (d). Detailed SEM photomicrograph of clinopyroxenes from Zone 2 (e). Detailed SEM photomicrograph of clinopyroxenes from Zone 1 (f).

Fig. 2. Compositional variations of clinopyroxenes from Zone 1 and Zone 2 expressed in terms of cations calculated on the basis of 6 oxygen atoms per formula unit and molecules, i.e. diopside (Di), hedenbergite (Hd), enstatite (En), ferrosilite (Fs), jadeite (Jd) and tschermakitic components (∑Ts equals to the sum of Ca-, CaFe-, CaCr- and CaTi-Tschermak molecules).

Fig. 3. Test for equilibrium of Mollo et al. (2013b) based on the difference (Δ) between diopside + hedenbergite (DiHd) contents measured in the analyzed crystals with those predicted for clinopyroxene via regression analysis of clinopyroxene-melt pairs at equilibrium. Data from this study plot within 10% of the one-to-one line, suggest near-equilibrium crystallization (a). Test for equilibrium of Putirka (2008) based on the Fe–Mg cation exchange reaction [$Kd_{Fe–Mg} = (Fe^{cpx} /$

Fe^{melt}) × (Mg^{melt}/Mg^{cpx})]. Clinopyroxene-melt pairs match with both the equilibrium ranges of 0.27 ± 0.03 and 0.28 ± 0.08 indicated by Putirka et al. (2003) and Putirka (2008) (b). Clinopyroxene crystallization temperatures estimated by the *P*-H_2O-independent thermometer of Putirka et al. (1996) with uncertainty ±23 °C (c).

Fig. 4. Compositional variations of melts from Zone 1, Zone 2, and Zone 3 corresponding to residual melt of the trachybasaltic lava, hybrid melt formed at the quartzite-lava interface, and SiO_2-rich melt resulting from partial dissolution of quartz grains respectively.

Fig. 5. Quantitative X-ray maps of the quartzite-lava interface showing progressive assimilation of the SiO_2-rich melt from quartz dissolution by the Etnean magma.

Fig. 6. Si-Al X-ray overlay map in which, among all major cations, silicon and aluminium show the greatest chemical variations.

Fig. 7. Linear least-squares mass balance calculations that couple the simple mixing process with clinopyroxene crystallization (cf. Barnes et al., 2002). The goodness of fit is corroborated by the low sums of squares of residuals.

Fig. 8. Partition coefficients from Zone 1 and Zone 2 presented as Onuma diagrams (Onuma et al., 1968) in which elements are grouped by ionic charge for M1 and M2 clinopyroxene crystallographic sites and arranged from smallest to largest ionic radius (Shannon, 1976) within each group.

Fig. 9. Partition coefficients D_{TE} (i.e., D_{Cr} and D_{Sc}), D_{HFSE} (i.e., D_{Hf} and D_{Zr}), D_{LILE} (i.e., D_{Pb} and D_{Sr}), and D_{REE+Y} (i.e., D_{La} and D_{Lu}) from Zone 1 and Zone 2 plotted against ^{T}Al.

Fig. 10. Lattice strain parameters calculated by the thermodynamically-derived model of Wood and Blundy (1997) are plotted against the aluminum content within the tetrahedral site of clinopyroxene (i.e., ^{T}Al) (a) and the number of non-bridging oxygens per tetrahedral cations in the melt (i.e., NBO/T) (b). D_0 is the partition coefficient for the strain-free substitution, r_0 is the radius of a hypothetical cation that substitutes into the site with zero strain, and E is the effective Young's modulus for the lattice site.

Fig. 11. Values of REE+Y (i.e., D_{La} and D_{Lu}) and HFSE (i.e., D_{Ti} and D_{Zr}) partition coefficients measured from this study are compared with those predicted by the models of Wood and Blundy (1997) and Hill et al. (2011), respectively. Linear regression fits of data yield high correlation coefficients (R^2) and low standard errors of estimate (SEE).

Fig. 12. D_0 values predicted for the partitioning of REE+Y during magma differentiation are plotted against T and ^{T}Al, and compared with the strain-free partition coefficients measured for Zone 1 and Zone 2 clinopyroxenes.

Fig. 13. Ce and Y (a), and Ti and Zr (b) partition coefficients as a function of temperature and clinopyroxene composition are used to illustrate magma dynamics driven by fractional crystallization (FC) and assimilation and fractional crystallization (AFC) processes.

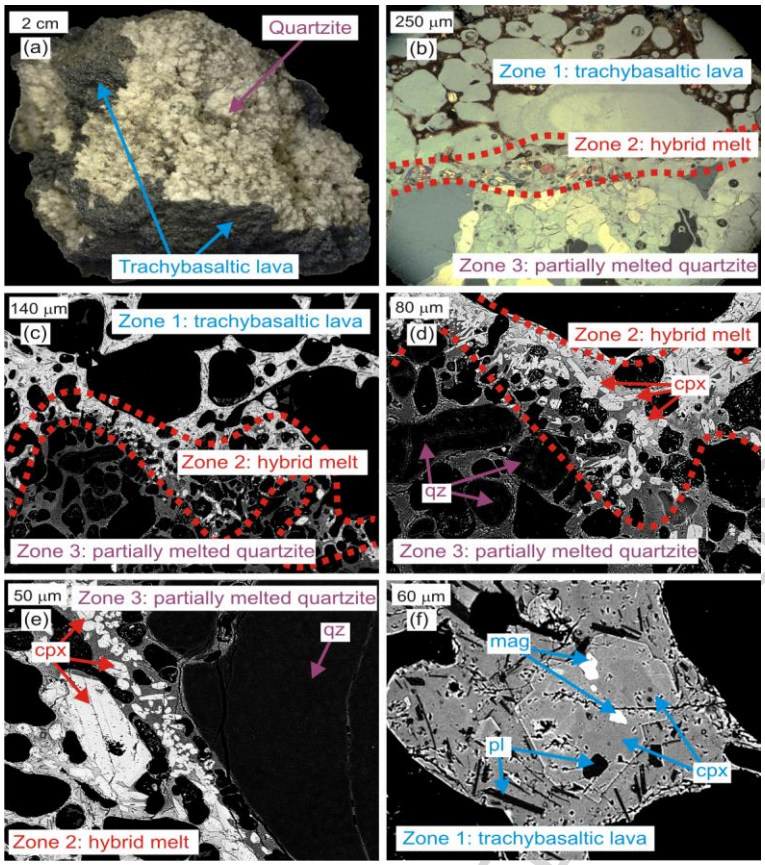

Figure 1

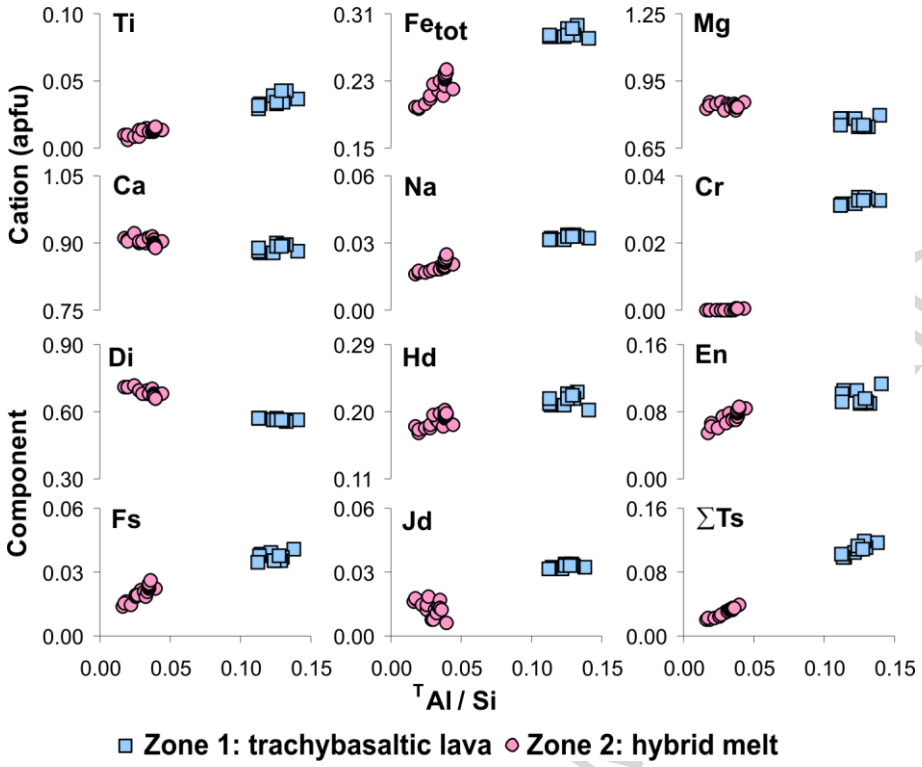

Figure 2

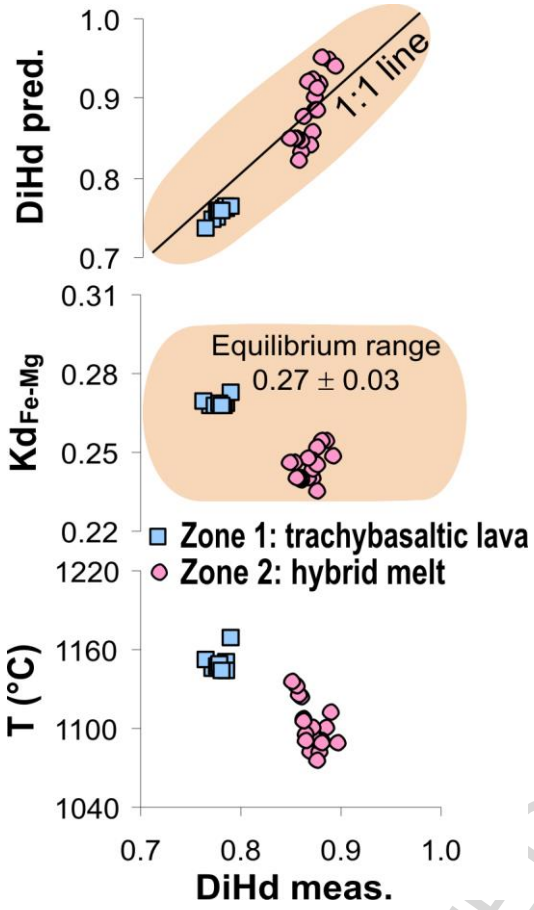

Figure 3

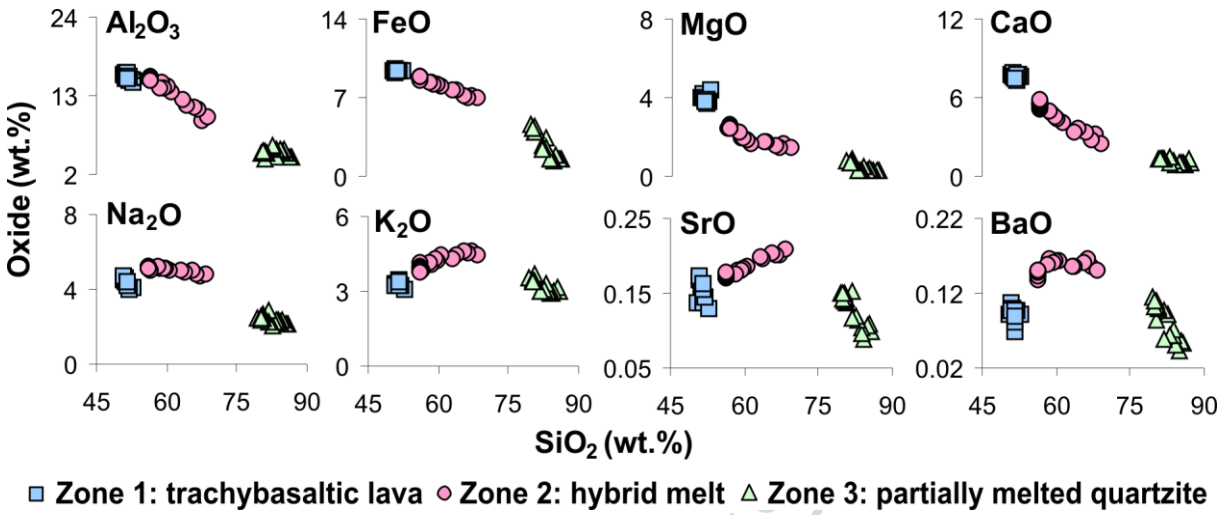

Figure 4

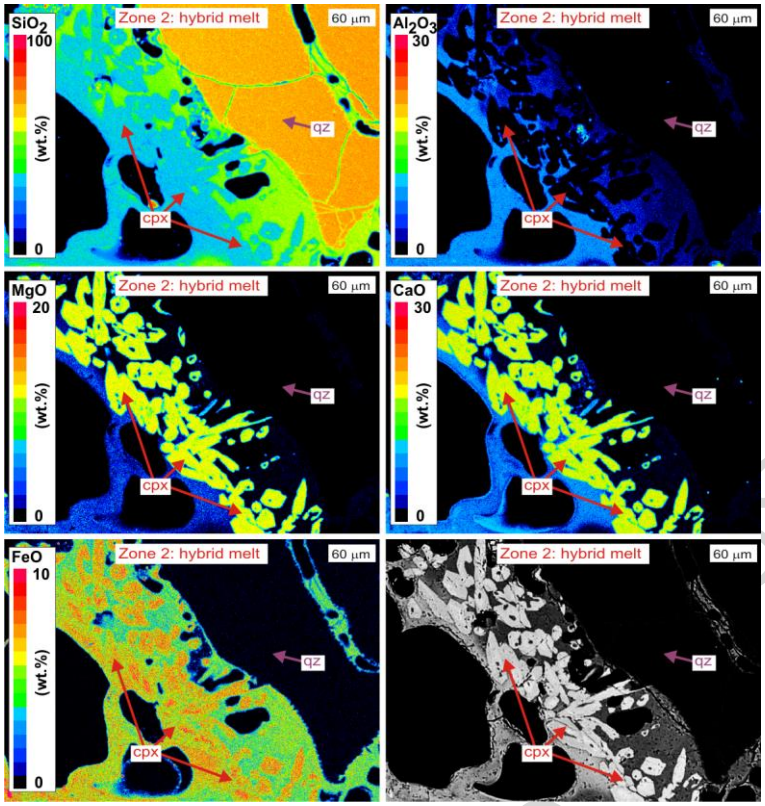

Figure 5

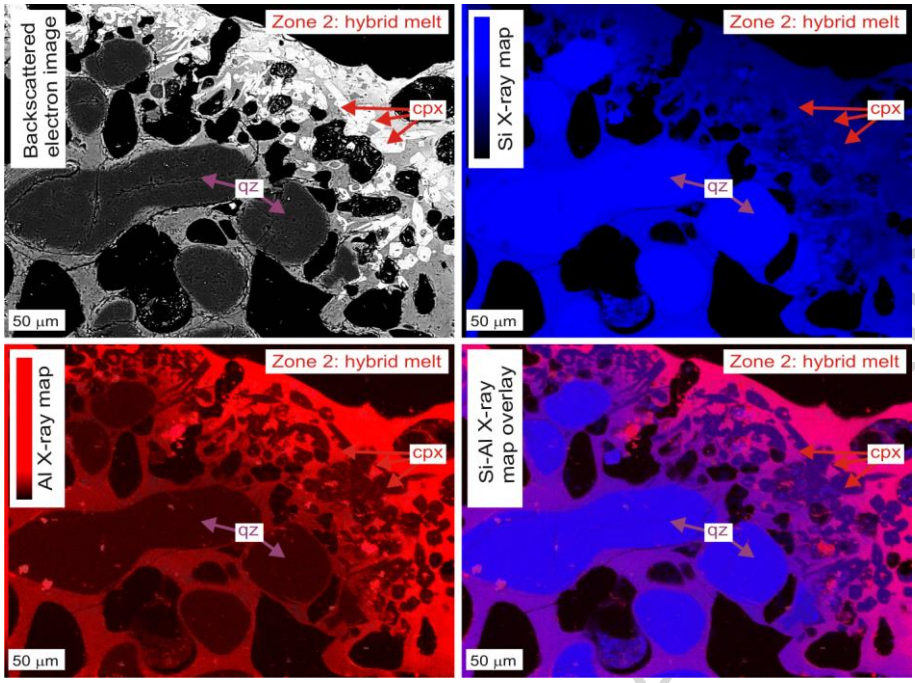

Figure 6

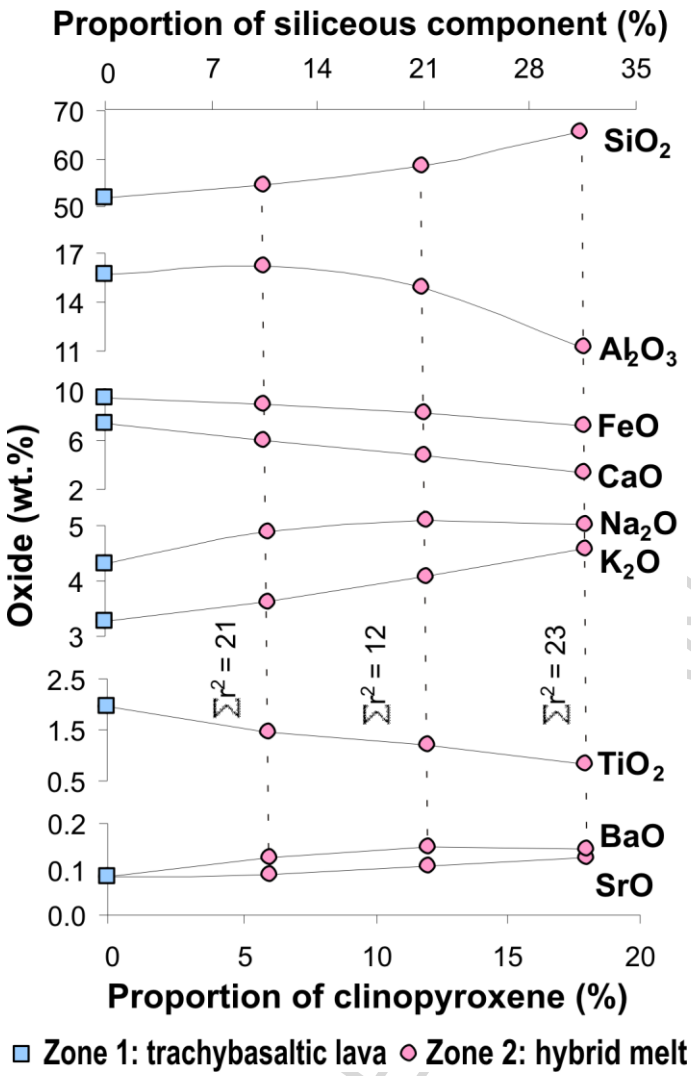

Figure 7

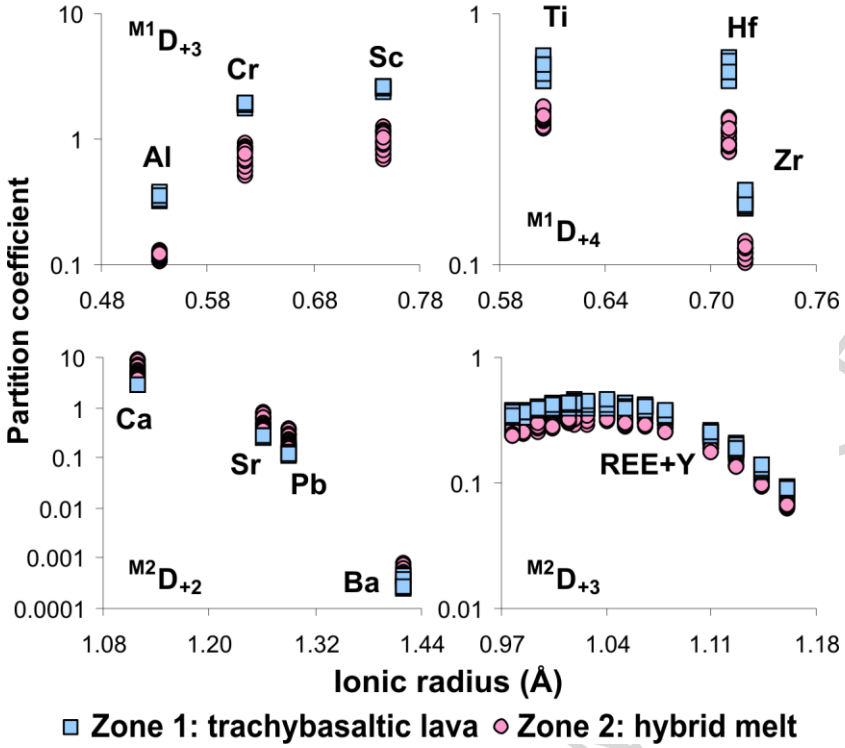

Figure 8

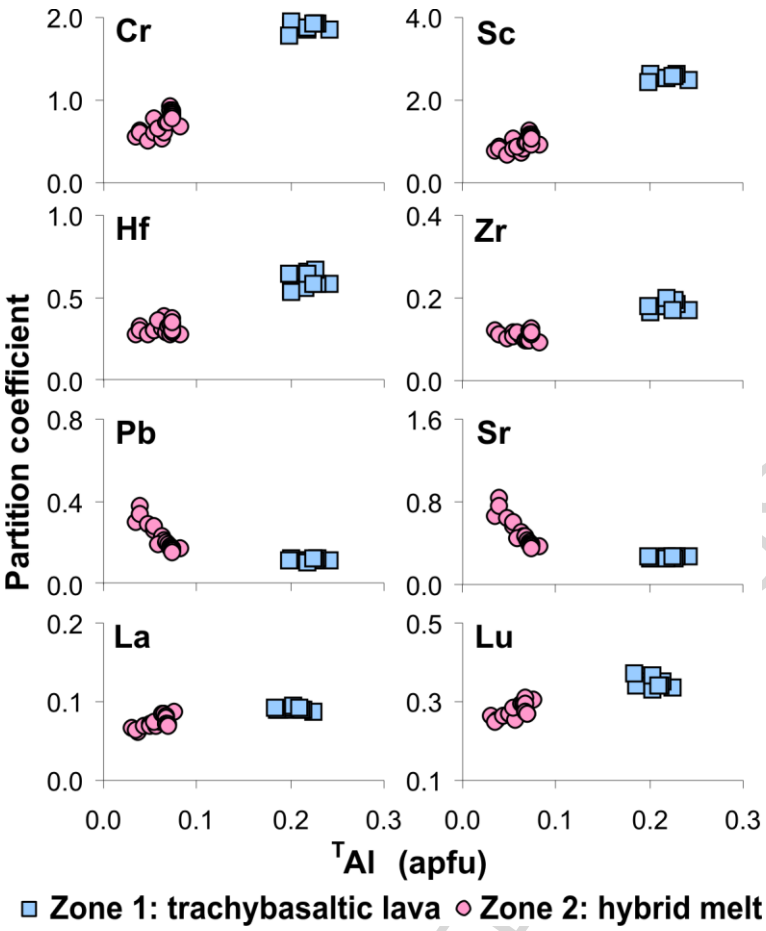

Figure 9

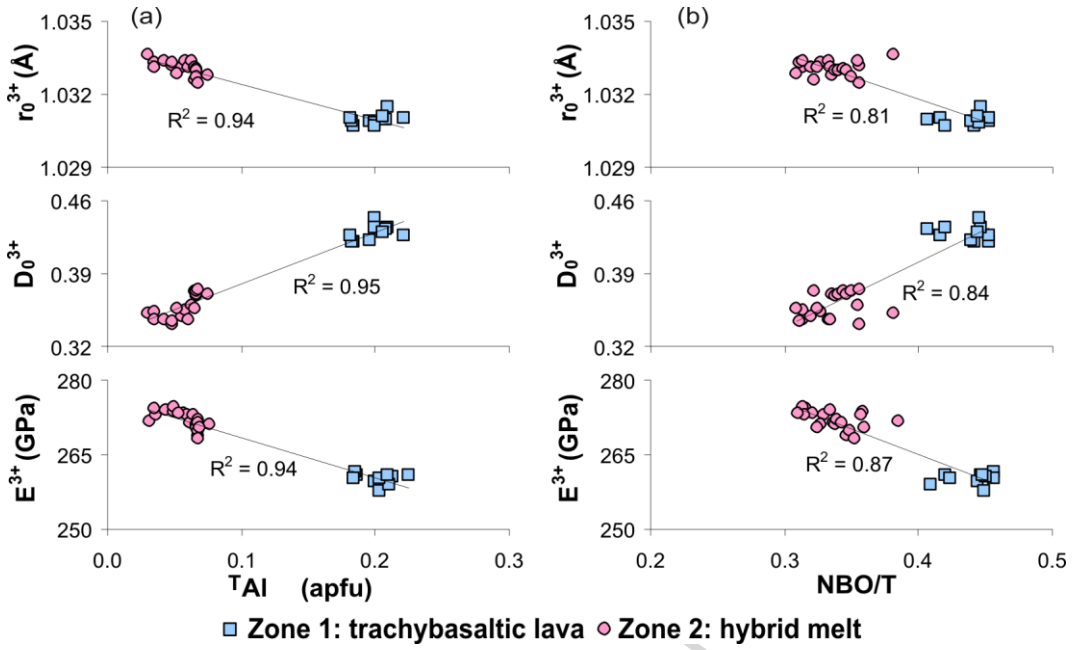

Figure 10

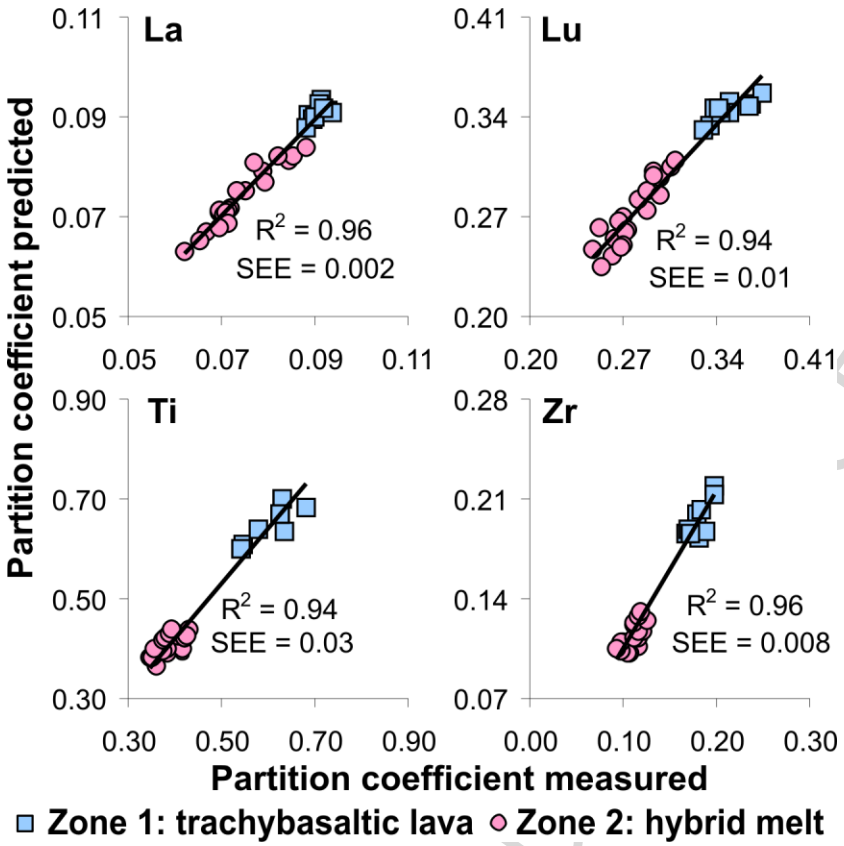

Figure 11

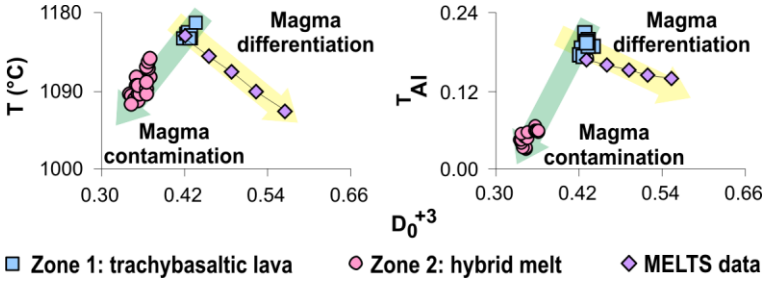

Figure 12

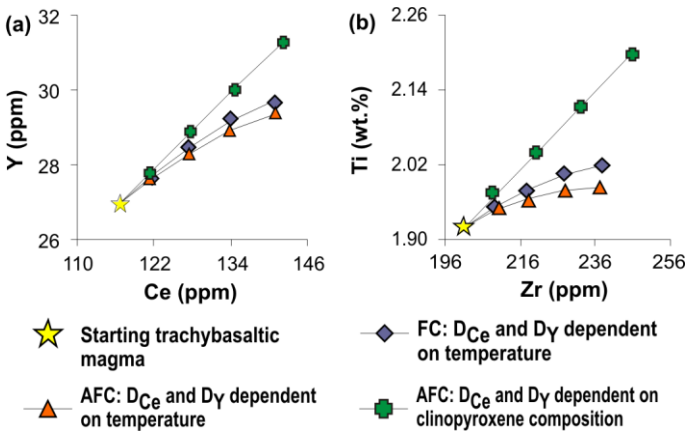

Figure 13

Research Highlights

Siliceous crustal xenoliths are sometimes erupted at Mt. Etna volcano > Magma contamination is accompanied by hybrid melts and newly-formed clinopyroxenes > Cation exchanges across the M1, M2, and T sites of clinopyroxene occur > Partition coefficients diverge from those derived by magmatic differentiation.